MECHANISMS THAT PROMOTE LIBERATION OF MITOTIC STRESS-INDUCED DEATH

Rebecca K. Sinnott

A dissertation submitted to the faculty of the University of North Carolina at Chapel Hill in partial fulfillment of the requirements for the degree of Doctorate of Philosophy in the Department of Pharmacology, School of Medicine.

Chapel Hill
2013

Approved by:

Angelique W. Whitehurst

Robert A. Nicholas

Stephen L. Rogers

W. Kimryn Rathmell

Mohanish Deshmukh

ABSTRACT

REBECCA K SINNOTT: Mechanisms that promote liberation of mitotic stress-induced death
(Under the direction of Dr. Angelique Whitehurst)

Paclitaxel is an anti-mitotic drug that, due to its success in the clinic, has become a backbone of first-line chemotherapeutic regimens for many malignancies including non-small cell lung cancer (NSCLC). While paclitaxel-based regimens are efficacious for some NSCLC patients, response is often incomplete, rarely curative and unpredictable, indicating widespread intrinsic resistance in chemo-naïve tumors. Thus, there is an unmet need for new combinatorial treatment strategies to better target paclitaxel resistant tumor cells.

To study the molecular basis for this resistance, we first established a test bed of NSCLC-derived cell lines that evade cell death from high concentrations of paclitaxel due to an uncoupling of mitotic damage from cell death. We then employed a genome-wide loss-of-function cytotoxic screen to identify the molecular components that can re-engage paclitaxel-mediated cell death programs in an otherwise paclitaxel-resistant background. This screen was performed in the presence and absence of a mitotic damaging, yet sub-lethal, dose of paclitaxel. This approach revealed a cohort of proteins that support tumor cell viability in the presence of mitotic damage.

From this study, we find that prolonging a mitotic delay, by inhibition of either the APC or novel mitotic regulators, CASC1 and TRIM69, collaborates with a sub-lethal dose of paclitaxel to engage cell death programs. In particular, we find that CASC1,

which is frequently co-amplified with KRAS, is essential for microtubule polymerization and mitotic spindle formation. We also identified TRIM69, an E3 ubiquitin ligase, that we find is recruited to the spindle poles during mitosis to support mitotic fidelity. Importantly, stable depletion of either CASC1, or TRIM69, attenuates tumor cell growth *in vivo*. Finally, we demonstrate that pharmacological inhibition of the APC collaborates with an otherwise sublethal dose of paclitaxel.

We hypothesize that during the course of tumor evolution, cancer cells become dependent on mechanisms that support rapid and inappropriate mitotic exit for cell viability and that these same intrinsic mechanisms are engaged to evade anti-mitotic therapeutics. Thus, therapeutic strategies that can prolong a mitotic delay may enhance patient response to paclitaxel-based therapies.

ACKNOWLEDGEMENTS

First and foremost, I would like to thank my mentor, Dr. Angelique Whitehurst, for taking on a student with minimal experience, and providing countless hours, guidance and resources to support me throughout my dissertation research. I am grateful for her persistence in shaping me into a young scientist and demonstrating how to attack a problem and examine it from all angles.

I would like to thank Gary Johnson, Rob Nicholas and Ken Harden for shaping an excellent Pharmacology department in which to receive doctoral training and for their guidance when I needed support as a student. I would like to thank Charlene Ross in the UNC-Animal Core that assisted me with my xenograft studies, and Noah Sciaky for conversation and support in learning how to use the BD Pathway. I would also like to thank my committee, including Dr. Robert Nicholas, Dr. Stephen Rogers, Dr. Mohanish Deshmukh and Dr. Kimryn Rathmell for their insights.

I would like to thank all members of the Whitehurst lab, past and present, but in particular Kimberly Maxfield, Patrick Taus, Josh Wooten and the honorary Whitehurst lab member, Kate White. These fantastic colleagues are a constant source of both scientific and personal support. They are always available to talk about a new idea or approach, trouble shoot an experiment, or just talk science. These colleagues have truly become a lab family without which my time in graduate school would have been much more difficult. Finally I would like to thank my family, friends and future husband for their constant, unwavering support.

TABLE OF CONTENTS

LIST OF TABLES

LIST OF FIGURES

LIST OF ABBREVIATIONS AND SYMBOLS

ALK	Anaplastic lymphoma kinase
ANAPC5	Anaphase promoting complx 5
APC/C	Anaphase promoting complex / Cyclosome
APL	Acute promyelocytic leukemia
BSA	Bovine serum albumin
BUB3	Budding uninhibited by benzimidazoles 3
BUBR1	Budding uninhibited by benzimidazoles R1
CASC1	Cancer susceptibility candidate 1
CDC20	Cell division cycle 20
cDNA	Complementary DNA
CTG	Cell titer glo
CTRL	Control
CTA(s)	Cancer-testis antigen(s)
DAPI	4’-6-Diamidino-2-phenylindole
DMSO	Dimethyl sulfoxide
DNA	Deoxyribonucleic acid
EGFR	Epidermal growth factor receptor
EGTA	Ethylene glycol tetraacetic acid
ELM4	Echinoderm microtubule-associated protein like-4
FDA	Food and Drug Administration
GAPDH	Glyceraldehyde-3-phosphate dehydrogenase
GFP	Green fluorescent protein

GFP-H2B	Green fluorescent protein conjugated to histone 2B
HAUS1	HAUS augmin-like complex, subunit 1
HBEC	Human bronchial epithelial cell
HECT	Homologous to E6Ap carboxy terminus
HEPES	4-(2-hydroxyethyl)-1-piperazineethanesulfonic acid
IACUC	Institutional animal care and use committee
MAD2	Mitotic arrest deficient-like 1
MAGE	Melanoma antigen
MAGEA4	Melanoma antigen family A, 4
MAP(s)	Microtubule associated protein(s)
MCC	Mitotic checkpoint complex
MCL-1	Myeloid cell leukemia sequence 1
MISP	Mitotic spindle positioning
MTOC	Microtubule organizing center
NCI	National Cancer Institute
NEXN	Nexillin (F-actin binding protein)
Noc	Nocodazole
NSCLC	Non-small cell lung cancer
NuMa	Nuclear mitotic apparatus protein 1
Pac	Paclitaxel
PARP	Poly(ADP-ribose) polymerase 1
PCR	Polymerase chain reaction
PDE3B	Phosphodiesterase 3B

PLK1	Polo-like kinase 1
PML	Promyelocytic leukemia
PP1	Protein phosphatase 1
PPP1R18	Protein phosphatase 1, regulatory subunit 18, phostensin
qRT-PCR	Quantitative Real-time polymerase chain reaction
RARα	Retinoic acid receptor, alpha
Rb	Retinoblastoma protein
RhoA	Ras homolog member, family A
RING	Really interesting new gene
RNA	Ribonucleic acid
ROCK	Rho associated coiled-coiled containing kinase
RPE1	Retinal pigment epithelial cell line 1
SAC	Spindle assembly checkpoint
SD	Standard deviation
SDS	Sodium dodecyl sulfate
SEM	Standard error of the mean
shRNA	Short hairpin RNA
siRNA	Small interfering RNA
TRIM69	Tripartite motif containing 69

Chapter I. Introduction

Lung cancer treatment

Lung cancer is the leading cause of cancer-related death in the United States [1]. This high mortality rate is partially attributable to the often late stage of disease progression at the time of diagnosis, which leaves patients with limited therapeutic options beyond standard cytotoxic therapies [2]. Technological advancements over the past 10-15 years have allowed for the identification of patient subsets that carry specific genetic mutations that can be targeted to improve individual patient outcome. Currently, the epidermal growth factor receptor (EGFR) and the recently identified fusion protein, EML4-ALK, are examples of tumor vulnerabilities that can be targeted to improve non-small cell lung cancer (NSCLC) patient survival [3].

Gain-of-function mutations in the tyrosine-kinase EGFR (epidermal growth factor receptor) have been identified in NSCLC tumors with varying penetrance in different ethnicities [4, 5]. Patients with an EGFR mutation can benefit from addition of specific inhibitors, erlotinib and gefitinib, in combination with the cytotoxic standard-of-care regimen [6-10]. In addition to EGFR mutations, a small subset of patients, 2 % - 7 %, have been found to have a mutant fusion protein between the tyrosine kinases EML4 (echinoderm microtubule-associated protein like-4) and ALK (anaplastic lymphoma kinase) [11, 12]. The ELM4-ALK fusion protein is targetable and has a predicted 50-60 % patient response rate [5, 13]. Despite the promise of these targeted therapies for small subsets of NSCLC patients, the vast majority of NSCLC tumors contain either currently

non-targetable oncogenic alterations, such as alterations to KRAS, or no known genetic lesion [5]. Thus, for a majority of patients, the current cytotoxic standard-of-care is the only available treatment option.

The current first-line, standard-of-care therapeutic regimen combines a DNA damaging reagent with the anti-mitotic paclitaxel [14, 15]. While this paclitaxel-based regimen has been shown to be efficacious, particularly in ovarian cancer, response in non-small-cell lung cancer has been notoriously poor with an approximate 30 % partial response rate at best [15-19]. Thus, there is an unmet need for new therapeutic approaches for treatment of NSCLC. Given the paucity of available targets for individualized therapy and the promise of taxane-based therapeutic regimens, novel therapeutic strategies that synergize with paclitaxel based treatment are in high demand.

Herein, I describe the undertaking of a genome-wide loss-of-function screen performed in a chemoresistant NSCLC-derived background in the presence of a damaging dose of paclitaxel. This screen was performed to uncover those molecular mechanisms that can disengage paclitaxel-mediated cell death programs. Therefore, a discussion on paclitaxel's known mechanism of action and current therapeutic challenges is warranted.

Paclitaxel as a mainstay cytotoxic therapy

In the 1960s, the National Cancer Institute (NCI) began a broad scale screening initiative to identify natural products from plant, microbial, or marine-derived extracts that contained anti-cancer activity [20]. This screening approach identified paclitaxel as an active compound from a plant-derived extract of the Pacific Yew tree [21, 22]. In the NCI's tumor screening process, paclitaxel was found to have antileukemic and tumor

inhibitory specific activity [22]. Given paclitaxel's initial identification as a tumor-inhibiting agent, clinical studies were performed in ovarian cancer. The standard-of-care for ovarian cancer at the time was a platinum-based cytotoxic reagent that met with limited success and intrinsic resistance [17, 21, 23]. Initial paclitaxel clinical trials reported an impressive therapeutic response with at least 30 % of patients demonstrating either a 50 % reduction in tumor volume or a complete clinical response [17]. Additionally, patients who had been resistant to the platinum-based therapy were responsive to paclitaxel treatment, setting the stage for combination therapy clinical trials [17, 24, 25]. In the late 1980s, paclitaxel was shown to be efficacious in the treatment of both advanced NSCLC and breast cancer and was approved by the Food and Drug Administration (FDA) for use in 1992 [21, 26, 27]. Since then, paclitaxel has become a mainstay of cytotoxic therapy and is broadly used as the first-line standard-of-care in ovarian, breast and non-small cell lung cancer.

Paclitaxel biological mechanism of action

Following the initial finding that paclitaxel was a potent anti-tumor agent, critical studies took place in order to understand it's mechanism of action. Early studies led to the observation that paclitaxel can have profound impacts on microtubule dynamics and assembly [28, 29].

Microtubules exist as hollow tubes composed of 13 protofilaments, formed by α/β tubulin heterodimers, that exhibit the unique property of dynamic instability. Dynamic instability is defined by several kinetic properties including: growth rate, shrinkage rate, frequency of depolymerization (catastrophe), frequency and rate of catastrophe rescues, and the duration of a "paused" state, during which no dynamic changes occur [30, 31].

The ability to rapidly alter microtubule kinetics is essential for many cellular processes including, but not limited to, protein and vesicle transportation, a cells motility and cell division. Paclitaxel alters microtubule dynamics by directly binding the β-subunit of the α/β tubulin heterodimer. Binding of paclitaxel promotes a morphological change in the α/β heterodimer that results in an increased affinity for a neighboring protofilament [32]. The resulting increased affinity makes microtubule depolymerization energetically unfavorable and thus supports overall microtubule stability [31]. The initial *in vitro* studies found that at saturating concentrations, paclitaxel binds β-tubulin in a 1:1 ratio and increases both microtubule stability and promotes microtubule polymerization [31, 32]. From these observations, paclitaxel is broadly classified as a microtubule stabilizing drug that at therapeutic doses functions by altering microtubule dynamics [31, 33, 34].

Shortly after the discovery of paclitaxel's tumor inhibitory properties, paclitaxel was shown to induce damage to the mitotic spindle and inhibit appropriate mitotic division [29, 35]. Proper formation of the mitotic spindle for a high fidelity mitosis is critically reliant on rapid and stochastic remodeling of the microtubule network [31]. Given the paclitaxel-mediated impact on microtubule dynamics, it follows that the primary biological target of taxol treatment is mitosis.

During mitosis, the interphase microtubule network must be broken down and reorganized in order to form a bipolar mitotic spindle. The spindle is formed by microtubules that emanate out from the centrosomes, or mitotic spindle poles, and in a rapid seek-and-find manner, attach to chromosomes at their kinetochores. Proper bi-polar microtubule-kinetochore attachment aligns chromosomes on the metaphase plate for equal division into identical daughter cells [36]. This process requires long periods of

microtubule growth and the ability to shrink if an attachment is not initially attained [31]. Further, inappropriate microtubule-kinetochore connections must depolymerize to avoid erroneous segregation [37]. Once a cell has aligned all chromosomes on the metaphase plate, the cell continues to rely on microtubule dynamicity to apply tension across the established mitotic spindle and physically pull aligned chromosomes apart [38, 39]. Thus, disruption of appropriate microtubule dynamics impairs formation of a bipolar mitotic spindle and creates mitotic stress. Mitotic spindle formation is monitored by the sentinel spindle assembly checkpoint (SAC) to prevent erroneous chromosomal segregation. Inhibition of bi-polar spindle formation prevents satisfaction of the SAC which will in turn delay mitotic exit and, ideally, the genomic damage that would result from incorrect chromosome segregation.

In summary, treatment with paclitaxel inhibits microtubule dynamics, disrupts mitotic spindle formation and results in prolonged engagement of the SAC, which delays mitotic division. A prolonged mitotic delay can lead to cell death signaling, imparting the therapeutic benefit of paclitaxel treatment. Although the SAC has been well studied, how a prolonged delay ultimately couples to cell death and why some tumors are more sensitive to SAC engagement than others is still largely unknown.

Spindle Assembly Checkpoint

The spindle assembly checkpoint delays mitotic exit until chromosomes have become properly aligned by the mitotic spindle. The delay is achieved through inhibition of the anaphase promoting complex/cyclosome (APC/C), an essential E3 ubiquitin ligase, until kinetochores have become attached to microtubules. Kinetochore-microtubule attachments are monitored through key sentinel proteins MAD2, BUBR1 and BUB3 that

assemble on the kinetochore in a dynamic mitotic checkpoint complex (MCC). The MCC inhibits APC/C activity by directly binding CDC20, an essential co-activator of the APC/C [40-42]. As kinetochore-microtubule attachments are established, the core MCC proteins, such as MAD2, are readily removed. Thus, the presence of MCC proteins at the kinetochore is interpreted as a lack of microtubule attachment [41, 43, 44]. Experiments inhibiting the APC/C and testing localization of MCC proteins at the kinetochore will be evaluated in chapters 4 and 5.

In a normal, non-transformed cell, the SAC remains engaged until microtubules establish connections with all kinetochores. Misalignment of a single unattached kinetochore has been shown to significantly delay cell cycle progression [45]. Once proper chromosome alignment has been achieved, the SAC is considered satisfied and CDC20 is released to activate the E3 ligase activity of the APC/C. The APC/C then polyubiquitylates key mitotic proteins, such as cyclin B1 and securin, marking them for degradation, which in turn allows for onset of anaphase (Figure 1) [41].

A prolonged mitotic delay indicates some level of genomic damage that cannot be readily resolved. Thus ideally, a prolonged mitotic delay will engage cell death programs to eliminate proliferation of damaged cells [31]. However, as evidenced by accumulation of aneuploidy cells, or cells with an uneven number of chromosomes, in greater than 90 % of solid tumors, the spindle assembly checkpoint is not fail-safe [46, 47]. In addition to the late stage at which many NSCLC patients are diagnosed, patients also exhibit variable and paltry responses to paclitaxel-based treatment [15-19]. This suggests that tumors have mechanisms by which to survive paclitaxel-induced mitotic damage and bypass cell death signaling from a prolonged mitotic delay. In order to elucidate novel therapeutic

entry points to collaborate with paclitaxel treatment we must first understand the current therapeutic challenges.

Current challenges for paclitaxel based therapies

Paclitaxel has been a mainstay cytotoxic therapy for over twenty years. While treatment with paclitaxel can be highly efficacious, it is subject to the same challenges as most drugs, namely side-effects and drug resistance. Briefly, the dose-limiting side effects of paclitaxel treatment are neutropenia and peripheral neuropathy. These main side effects are accompanied by nausea, vomiting, alopecia and cardiac abnormalities [48]. Thus, even in paclitaxel-responsive patients, treatment regimens are limited due to the systemic effects on the patient. If mechanisms are identified that can synergize with paclitaxel treatment, one potential benefit could be reduction of the negative side-effects for the patient allowing for more aggressive treatment with lower doses of the cytotoxic drugs.

Resistance to paclitaxel treatment, both intrinsic and acquired, is common and can be achieved through several avenues [49, 50]. First, altering the propensity of a cell to induce apoptosis, thereby increasing general drug resistance, can dampen paclitaxel's cytotoxic effects [51]. A second avenue to resistance is through over-expression of drug efflux pumps, which can limit the ability of paclitaxel to accumulate in the cell [52]. Mutations to tubulin, or the paclitaxel binding site on tubulin, are rare [53] however, alterations to microtubule dynamic instability, altering paclitaxel's functional target, have been observed.

The degree of dynamic instability of a microtubule network is regulated by multiple factors, including the expression of varying tubulin isotypes [54]. There are six

α-tubulin and seven β-tubulin isotypes that can form heterodimers in multiple combinations. β-tubulin isotypes have been demonstrated to impart different degrees of dynamic instability [54, 55]. An increased expression of βIII-tubulin, which may decrease microtubule dynamicity, has been reported in models of acquired resistance in NSCLC and is associated with resistance to microtubule-targeted drugs in a number of epithelial cancers [34, 54, 56]. Altering microtubule stability could impact the availability of paclitaxel's biological target and diminish overall drug efficacy. Resistance to paclitaxel treatment can also be achieved through an uncoupling of paclitaxel-induced mitotic damage from cell death. While the mechanisms underlying mitotic stress-induced cell death are not well understood, the process of mitotic slippage allows cells to bypass the SAC and exit mitosis despite having a damaged mitosis or unaligned chromosomes. Thus, mitotic slippage may represent a fulcrum between mitotic cell survival and death.

Mitotic slippage

While the mechanisms of how anti-mitotic drugs produce a mitotic delay have been well studied, how cells ultimately respond to the prolonged mitotic delay is not well understood [49]. Elegant live-cell imaging studies have demonstrated that both the duration of mitotic delay and fate of arrested cells in response to mitotic stress is highly variable within and between tumor cell lines [57]. A prolonged mitotic delay may result in several distinct cell fates: cells may compensate and exit normally into two daughter cells, undergo apoptosis from mitosis, exit mitosis without dividing, or undergo what is termed mitotic slippage, which is the inappropriate segregation of unaligned chromosomes. This inappropriate mitotic slippage results in the formation of multi or micronucleated cells. The fate of micronucleated cells is also highly variable. They may:

undergo apoptosis in the following G1 due to their sustained genomic damage, exit the cell cycle, or continue to undergo additional rounds of division [57, 58] (Figure 2). It was originally thought that the ability of cells to aberrantly exit mitosis would be due to wide spread mutation or loss of core SAC proteins; however, this was found to be a fairly rare event [59]. While the mechanisms governing these various responses are not clearly defined, mitotic slippage has been suggested to be the result of competing kinetic mechanisms engaged upon entry into mitosis.

Cyclin B1, a substrate of the APC/C^{CDC20} , must be degraded in order to progress from metaphase to anaphase [41]. To address the question of how cells are able to inappropriately exit mitosis without proper chromosome alignment, Brito et al designed a GFP-cyclin B1 lacking a D-box, the recognition sequence for ubiquitination by the APC/C^{CDC20} [60]. This APC/C^{CDC20} resistant cyclin B1 construct was stably expressed in human RPE-1, non-tumorigenic cells, to monitor cyclin B1 stability in response to various mitotic insults [60]. Through this study, Brito et al found that in the presence of an active spindle assembly checkpoint, cyclin B1 is slowly degraded despite it not being targeted by APC/C^{CDC20}. This study suggests that the APC/C is not fully inhibited by the SAC and a low level of constant ubiquitination allows for the slow degradation of cyclin B1 over time [60]. The hypothesis that the APC/C is not fully inhibited while the SAC is active is supported by additional lines of evidence. Several APC/C substrates have been shown to be degraded in a CDC20 dependent manner in the presence of an active SAC including CDC20 itself [61-64]. These data demonstrate that a low level of APC/C activity both reinforces the SAC-mediated mitotic delay, by targeting CDC20, and supplies a timing mechanism to allow cells to eventually escape a mitotic delay, by

targeting cyclin B1.

In addition to slow degradation of cyclin B1, MCL-1, (myeloid cell leukemia sequence 1) a pro-survival protein, is targeted for degradation by both APC/C^{CDC20} dependent and independent mechanisms during a prolonged mitosis [65, 66]. It is posited that once a threshold of pro-apoptotic signals, such as the loss of MCL-1, accumulate, a cell will irreversibly commit to cell death programs. If sufficient cyclin B1 is degraded to allow for mitotic exit after the death threshold has been crossed, the cell may still undergo apoptosis in the resulting G1 [57, 67]. Thus, cell fate may be intimately tied to mitotic timing. However, the mechanisms ultimately coupling mitotic timing and mitotic damage to cell death have not been elucidated.

Currently the molecular mechanisms that govern the capacity to slip through a prolonged mitotic arrest are of high interest. Understanding those mechanisms that allow a tumor cell to uncouple mitotic stress from cell death, independent of other known resistance mechanisms, can lead to improved combinatorial strategies to improve taxane based therapies.

Project summary

The ultimate goal of the project described herein has been to elaborate the molecular mechanisms that support tumor cell survival in the presence of mitotic damage. To this end, we first characterized a cohort of NSCLC-derived cell lines for paclitaxel responsiveness to identify a paclitaxel-resistant discovery platform. From an identified cohort of resistant cell lines, the HCC366s were selected in which to perform a genome wide, siRNA-based, loss-of-viability screen in the presence and absence of a damaging, yet sub-lethal dose of paclitaxel. Importantly, this cell line contains neither

tubulin mutations nor an increased expression of the multi-drug efflux pump MDR-1 (unpublished observation). Performing the screen both in the presence and absence of paclitaxel allowed for the identification of those molecular components that are specifically required to deflect mitotic stress-induced cell death. Secondary screening analysis coupled a medium through put cytotoxicity screen with a live-cell imaging platform. This strategy allowed stratification of high-interest chemosensitizers and revealed a cohort of proteins that support both tumor cell viability and mitotic slippage. We identify ANAPC5, a core component of the APC/C, whose genetic and pharmacological inhibition collaborates with paclitaxel treatment. Further we find that tumor cells are more sensitive to direct APC/C inhibition than normal cells suggesting that targeting mitotic timing may have a targetable therapeutic window.

The other members of the mitotic slippage cohort had never before been implicated in mitosis. Specifically, we identified CASC1 and report it functions as a novel regulator of microtubule dynamics and the E3 ubiquitin ligase, TRIM69, as a novel component of mitotic spindle poles. Overall, this work supports the hypothesis that prolonging a mitotic delay through targeting SAC activity and mitotic exit can recouple mitotic damage to cell death. From this work, we hypothesize that tumor cells rely on mitotic slippage mechanisms as a means of evading mitotic stress-induced cell death. Those cells that have evolved mechanisms to undergo a rapid and inappropriate mitotic exit gain the collateral advantage of an intrinsic resistance to microtubule-targeted therapeutics.

Figure 1.

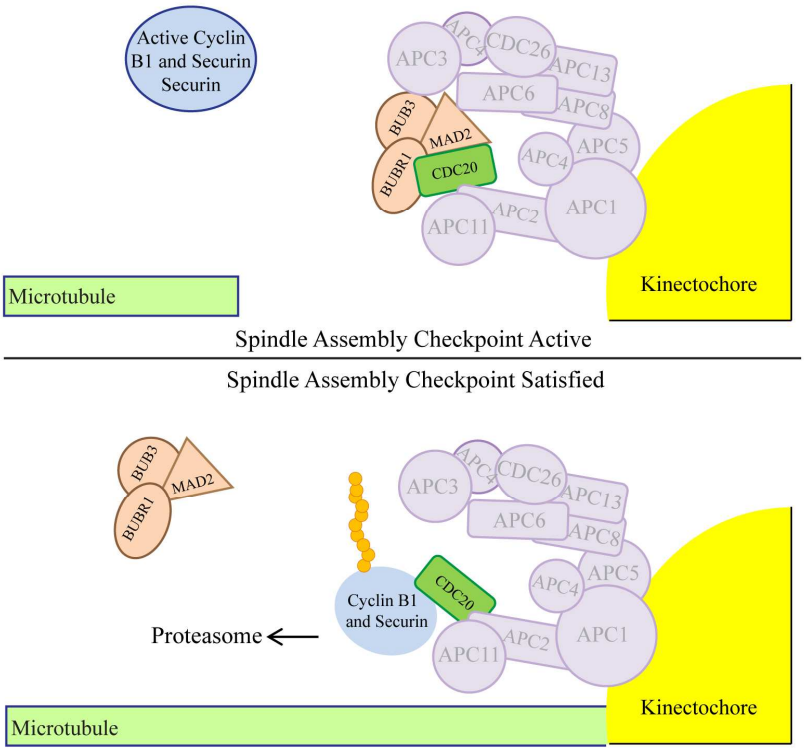

Figure 1. The spindle assembly checkpoint

The spindle assembly checkpoint is active at the start of mitosis in order to monitor the formation of the bipolar mitotic spindle. Top: The mitotic checkpoint complex (MCC-orange) is composed of MAD2, BUBR1 and BUB3. In the absence of a microtubule-kinetochore attachment, the MCC binds and inhibits CDC20. CDC20 is an essential activator of the APC/C E3 ubiquitin ligase (purple), thus binding of the MCC to CDC20 prevents activation of the APC/C. Bottom: Once a full bipolar mitotic spindle is formed and all kinetochores are attached to microtubules, the SAC is considered satisfied. When microtubules become attached to kinetochores and tension is established across the forming spindle, the MCC is released from CDC20 and removed from the kinetochore. CDC20 can then activate the E3 ligase activity of the APC/C and target key mitotic proteins, including cyclin B1 and securin, for proteasomal degradation. This allows the cell to progress from metaphase into anaphase.

Figure 2.

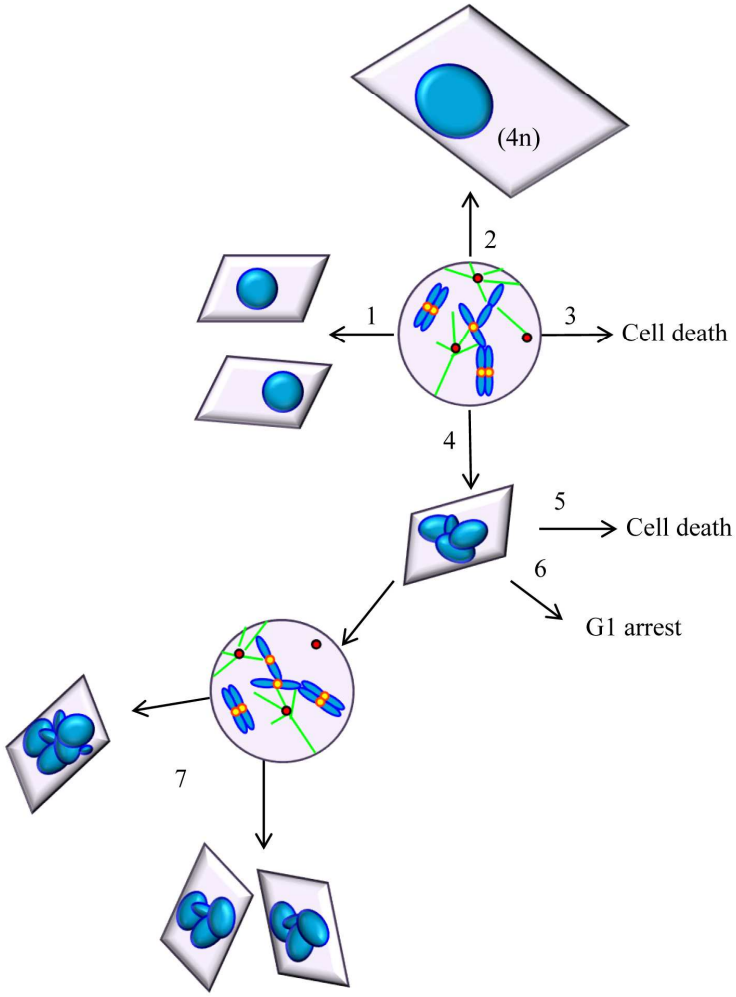

Figure 2. Variable fates following a prolonged mitotic delay.

Map of potential fates following a prolonged mitotic delay. Cells may (1) eventually align and exit into two normal daughter cells (2) exit mitosis without division (3) undergo cell death from mitosis or (4) aberrantly exit into a micronucleated cell(s). Micronucleated may cells die (5) from their incurred damage (6) enter into a G1 cell cycle arrest or (7) undergo additional rounds of division.

Chapter II. Materials and Methods1

Cells and Reagents: HBEC and NSCLC cell lines, except A549, were a gift from John Minna, 293s, A549s and HeLas were a gift from Dr. Michael White at UTSW. HBEC cell lines were maintained in keratinocyte medium supplemented with supplied epidermal growth factor and bovine pituitary extract (Gibco). HeLa and 293 cells were maintained in DMEM (Gibco) supplemented with 10 % FBS. NSCLC cell lines were maintained in RPMI medium (Gibco) supplemented with 5 % fetal bovine serum (FBS). Paclitaxel (Sigma or Tocris), Nocodazole (Calbiochem) and ProTAME (Boston Biochem) were dissolved in Dimethyl Sulfoxide (DMSO). APO-ONE® and Cell-Titer Glo® (CTG) were obtained from Promega.

Paclitaxel Dose Curves: Cell lines were seeded in 96-well plates at densities such that they reached 50 % confluence 48 hours later. 48 hours post-plating, cells were treated with indicated concentrations of paclitaxel. 48 hours post drug exposure, cell viability was assessed by Cell-Titer Glo® assay (Promega).

Immunofluorescence: Immunofluorescence was performed as previously described [68, 69]. Briefly, cells were grown on coverslips in 24-well plates. Cells were [1]fixed in either 3.7 % formaldehyde, or methanol, permeabilized with 0.5 % Triton X-100 and blocked in a solution of PBTA: 1X PBS, 1 % Tween-20 and 5 % w/v Bovine Serum Albumin (BSA). For microtubule preservation (Figure 3D), cells were pre-extracted in

[1] Elements of the work referenced in this chapter are under review for publication in:
Sinnott R et al., Mechanisms that promote the liberation of mitotic-stress induced tumor cell death. (in submission) Cancer Research

BRB80 (80 mM PIPES pH 6.8, 1 mM $MgCl_2$, 5 mM EGTA) and 0.5 % Triton X-100 for 30 seconds, fixed in 0.5 % gluteraldehyde and quenched with 0.1 % sodium borohydride. Primary antibody incubations were performed in PBTA for 1 hour or overnight. Secondary antibodies were Invirogen Alexa Fluor (488, 546 and 648) conjugated anti-mouse or anti-rabbit and used at a dilution of 1:2000 for 30 minutes at 37°C. Cells were then washed and mounted using ProLong® Gold AntiFade with 4',6-diamidino-2-phenylindole (DAPI) reagent (Invitrogen). Mitotic index was scored as the % of cells in mitosis by manual inspection using phospho-H3B (Ser10) and/or DAPI stain for condensed chromatin. Slides were imaged on an Axioimager upright microscope (Zeiss) equipped with a charge-coupled device (CCD) camera.

Immunoblotting: Cells were lysed in boiling 2X Laemmli sample buffer as previously described [68, 69]. The primary antibodies used were from Santa Cruz (GAPDH, CASC1, PDE3B, Actin, Rabbit Myc-A14, Mouse Myc-9E10, GST), Epitomics (Cleaved Caspase-3), Covance (MAD2L1), Abgent (TRIM69, MAGE-A4), Sigma (β-tubulin), Abcam (Pericentrin), Roche (HA), and Millipore (phospho-histone-H3 (ser10)).

Stable cell line production: Cell lines stably expressing myc-TRIM69A or green fluorescent protein-histone H2B (GFP-H2B) were generated by retroviral transduction. Retrovirus was produced by transfection of 293GP cells with vesicular stomatitis virus G protein (VSV-G) and either pLPCX-myc-TRIM69A or pCLNCX-H2B-GFP (gift from Dr. Gray Pearson at UTSW). Cells were infected with virus overnight and transduced cells were selected with puromycin (pLPCX-myc-TRIM69A) or geneticin (pCLNCX-GFP-H2B).

cDNA expression and plasmids: Cells were transfected with cDNA expression

vectors using Lipofectamine 2000 (Invitrogen) or Fugene 6 (Promega) according to the manufacturer's protocol. Plasmids used: Tomato-H2B, pCMV-myc (Clontech), pCMV-myc-TRIM69A, pCMV-myc-TRIM69B and pCMV-myc-TRIM69A (C50S/C53S).

High-content live–cell imaging: Cell lines were transduced with green fluorescent protein-histone H2B (GFP-H2B) using retrovirus mediated gene delivery as previously described [68-70]. Cells were imaged on a BD Pathway 855 imager using a 20x high numerical-aperture objective [68, 69]. Single-cell lineage tracing was performed as previously described [68, 70]. Briefly, individual cells undergoing mitosis were monitored for mitotic transit time, which was calculated as the time between nuclear envelope breakdown and DNA decondensation. Mitotic fate was defined as either generation of two daughter cells, mitotic death or micronucleation. Nuclear blebbing and pyknotic nuclei that ceased to move were considered dying cells.

siRNA Transfection: Reverse transfections conditions were performed as previously described [68, 69]. Control siRNA transfections were performed with either (Dharmacon) a pool targeting DLNB14 or a non-targeting siRNA pool [68-71].

shRNA Infections: Lentiviral pLKO.1 vectors expressing short hairpin RNA (shRNA) were obtained from The RNAi Consortium TRC) (http://www.broadinstitute.org/rnai/public) through Open Biosystems. Virus was generated according to manufacturer protocol. 1×10^6 HCC366 cells were infected for 12 hours and target mRNA knockdown was assessed 72 hours post infection by qPCR as indicated above.

Tumor Xenografts. pLKO.1 vectors expressing short hairpin RNA (shRNA) were used to generate lentivirus to infect HCC366 cells. Target knockdown was assessed

72 hours post-infection. Cells were collected 96 hours post-infection and 2 $x10^6$ cells were injected into the flank of female NSG (NOD.Cg-Prkdc^{scid} Il2rg^{tm1Wjl}/SzJ JAX®) mice. 3 $x10^6$ non-transduced cells were used for taxol studies. All mice were housed in sterile conditions according to an approved IACUC protocol and abiding by all UNC Animal Welfare guidelines. Tumor growth was monitored by caliper measurement at indicated time points. Overall health of mice was monitored regularly according to IACUC regulations. When tumor burden met IACUC limits or earlier, mice were sacrificed and tumors fixed in formalin. In paclitaxel experiments, mice were treated with 20 mg/kg of paclitaxel 10 days post injection, at a frequency of two days per week for 4 weeks.

Hematoxylin and eosin staining (H&E): Tumors from xenograft mouse studies were excised, formalin fixed and paraffin embedded. Tissue was processed by routine microtomy into 5-6 micron sections for automated staining.

siRNA screen: A genome-wide siRNA screen was performed in a 96 well format using a previously described Thermo-Fisher library targeting 21,127 unique genes [71]. A two-condition, triplicate analysis screen was performed in which HCC366 cells were transfected with siRNAs for 48 hours, followed by exposure to either vehicle or 10 nM paclitaxel for an additional 48 hours. Cell viability was then measured using Cell Titer Glo®. The screening protocol was identical to that previously described with the following exceptions: HCC366 cells were used at a final number of 1x 10^4, HCC366 cells were transfected with Dharmafect 2 complexed siRNAs in RPMI serum free medium and cells were treated at 48 hours post-transfection with either vehicle or paclitaxel and a final FBS concentration of 10 % [71].

Quantitative PCR (qPCR): Cells were transfected with siRNAs for 72 hours. Total RNA was collected using the GenElute Mammalian Total RNA Miniprep Kit (Sigma). 2 µg total RNA was used in subsequent reverse transcription using the High-Capacity cDNA reverse transcription kit (Applied Biosystems). Quantitative reverse transcription PCR (qRT-PCR) was performed with TaqMan gene expression assays and ribosomal protein L27 (RPL27) was used as the endogenous control. Probes spanned exon boundaries to avoid genomic contamination. The ddCT method was used to calculate relative amounts of mRNA.

Colony formation assays: $1x10^5$ HCC366 cells were reverse transfected with Dharmafect 2 in 24 well plates with either control or target siRNAs. 48 hours post-transfection, cells were treated with either vehicle control or 10 nM paclitaxel. 96 hours post transfection $2x10^3$ cells were trypsinized, counted in the presence of trypan blue, and replated in 6 well format. Cells were fed biweekly and monitored for up to 3 weeks. Cells were then fixed with 3.7 % paraformaldehyde and stained with Geimsa. Colonies were counted manually.

Microtubule Regrowth Assay – Cells were reverse transfected and seeded at $2x10^4$ (H1299) or $5x10^4$ (HBEC). Seventy-two hours post transfection cells were exposed to 11µM nocodazole for 1 hour to assure complete depolymerization. Cells were then washed once with PHEM buffer (60 mM PIPES, 25 mM HEPES, 10 mM EGTA, 2 mM, $MgCl_2$, 1 M Paclitaxel) and allowed to regrow for indicated time. Cells were then permeabilized with 0.5 % Triton-X-100 for 1 min. Cells were subsequently fixed and immunostained as detailed above.

***In vivo*-polymerized tubulin assay.** H1299s were reverse transfected and seeded

at 1.5 x 10^5. 72 hours post transfection cells were rinsed in PBS and lysed in microtubule stabilizing buffer (100 mM PIPES, 2 M glycerol, 0.1 M MgCl2, 2 mM EGTA, 0.5 % TritonX-100, 5 µM Paclitaxel). Aliquots of whole cell lysates were collected and the remaining lysates were centrifuged for 30 minutes at 4°C and 16,000 RCF. The supernatant (monomeric tubulin) was collected and pellet (polymerized tublin) resuspended in microtubule stabilizing buffer. Lysates were then analyzed by immunoblot.

Analysis of Gene Expression Data Sets: Evaluation of CASC1 expression in The Cancer Genome Atlas datasets was performed through the CBioPortal [72]. Lung adenocarcinoma, breast and ovarian cases were provisional microarray data sets deposited by TCGA. Lung Squamous cases were previously reported [73]. Expression cutoff were based on z-score threshold of +/- 2. Odds ratios were also calculated by cBio Portal.

Immunoprecipitation: 293T cells were transfected in 3 µg of cDNAs using FuGENE®6. 24 hours post-transfection cells were lysed in a non-denaturing lysis buffer (20 mM TRIS pH 7.4, 50 mM KCl, 1 % NP40 and protease inhibitors (Sigma)). Following a 16,000 RCF spin for 30 minutes, soluble cell fractions were isolated and precleared with protein A/G beads (Invitrogen) and mouse or rabbit IgG for 1 hour. Lysates were then incubated with protein A/G beads for 3-5 hours with 1 µg antibody or control IgG. Beads were subsequently washed (3 x 5 min) in lysis buffer. Bound proteins were released from A/G beads into 2x Laemelli sample buffer and resolved via SDS-PAGE gel followed by immunoblotting.

Protein Purification: Recombinant pGEX4T1-GST-TRIM69A was expressed in

E.coli (BL21) in the presence of $ZnCl_2$. Bacteria were lysed with protein buffer (50 mM, Tris pH 7.7, 150 mM KCl, 0.1 % Triton X-100, 1 mM DTT) supplemented with lysozyme. GST-TRIM69A was isolated using glutathione-agarose (Sigma) and eluted with protein buffer supplemented with glutathione.

***In vitro* auto ubiquitinylation assay:** The Enzo® Auto-ubiquitinylation kit was used to evaluate GST-TRIM69A for ubiquitinylation activity. Briefly, 0.1 µM ubiquitin activating enzyme (E1), 0.05 µg UbcH5b (E2) and 1µg recombinant GST-TRIM69A were incubated with 1 mM DTT, 5 mM Mg-ATP, 3 µg Flag-ubiquitin, 20 µg bovine ubiquitin and ubiquitin buffer (Enzo). Ubiquitinylation assay was maintained at 30°C for two hours and quenched by addition of 2x Laemelli buffer followed by incubation at 95°C for 5 minutes. Negative control reactions were performed in the absence of E2 enzyme.

Chapter III. Genome wide loss of function screen uncovers novel modulators of mitotic slippage

Defining a screening platform for paclitaxel resistance.

Paclitaxel-based treatment has been fairly successful in ovarian patients; however response in NSCLC has been notoriously variable. The current standard of care, a combination paclitaxel and platinum-based cytotoxic regimen, results in a 30 % partial response at best with few to no patients exhibiting a complete response [15-19]. The molecular basis for this widespread intrinsic chemoresistance is not currently understood, however it can be recapitulated in NSCLC-derived cell lines. Exposing a panel of NSCLC-derived cell lines to escalating doses of paclitaxel reveals a cohort of chemoresistant cell lines, the HCC366, HCC1171, H2887 and HCC515s, that show minimal loss of viability in response to up to 1 μM paclitaxel (Figure 3A and B). While this cohort is able to evade apoptosis at high doses of paclitaxel, a low, clinically relevant dose of 10 nM is sufficient to produce abnormal mitotic spindles and the accumulation of micronucleated cells (Figure 3C). These observations indicate that although these cells are considered ‘resistant’, paclitaxel is hitting its biologically relevant target. This mitotic damage response was observed in all members of the resistant cohort as assessed by nuclear morphology (Figure 3D).

Live-cell imaging of HCC366 cells engineered to express GFP-histone 2B, revealed a concentration dependent mitotic delay that was rescued by depletion of core SAC proteins MAD2 and BUBR1 (Figure 3E). Together, these data indicate that SAC

signaling remains intact and these resistant cells are capable of sensing and responding to mitotic stress. Although the SAC remains functional, micronucleated cells begin to accumulate at low doses of paclitaxel with a uniform mitotic slippage response at higher concentrations. In contrast, the paclitaxel-sensitive H1155 cell line undergoes a dramatic mitotic delay that resolves as either mitotic death or aberrant exit when treated with a damaging dose of paclitaxel (Figure 3E and F). Thus, paclitaxel-resistant HCC366 cells possess the capacity to bypass the SAC and may be considered a slippage-prone cell line. Further, live-cell imaging studies revealed that a majority of micronucleated HCC366 cells are able to survive for up to 40 hours, post-mitotic slippage. Approximately 8 % of the micronucleated cells underwent apoptosis and 8 % underwent an additional round of division (Figure 3G). Together, these data indicate that mitotic damage has become uncoupled from tumor cell death.

Finally, HCC366 cells were used to establish a xenograft mouse model to determine if the mitotic slippage event occurs *in vivo.* Indeed, micronucleated cells were found to accumulate in tumors following systemic treatment with 20 mg/kg paclitaxel (Figure 3H). Given the robust and uniform micronucleation response and resistance to cell death from high doses of paclitaxel, HCC366 cells represent an ideal screening platform to identify molecular components whose depletion will recouple mitotic stress to cell death.

Genome wide loss of function screen

In order to identify the molecular components and mechanisms capable of uncoupling mitotic stress from cell death in an unbiased manner, we performed a genome wide siRNA screen in the presence and absence of a mitotic-damaging, yet sub-lethal,

concentration of paclitaxel (Figure 4A). This screen was performed by Angelique Whitehurst at UTSW using a Dharmacon siRNA library. The siRNA library, targeting over 21,000 genes, is arrayed in 96 well master plates, with each well containing a pool of 4 independent oligos targeting a single gene in the genome. Each library master plate was transfected in sextuplet allowing three replicates to be treated with vehicle and three replicates to be treated with 10 nM paclitaxel 48 hours post transfection. The concentration of paclitaxel was chosen because it is a damaging yet sublethal dose at which HCC366 mitotic cells uniformly undergo mitotic slippage from a brief delay. Forty-eight hours post treatment, wells were assessed for cell viability using the luminescent Cell-titer-glo assay, which measures total ATP. The raw luminescence values were normalized to the median values in each row to correct for any position effects. The raw data was manually cleaned by Angelique Whitehurst to remove any siRNA pools whose replicate values had a greater than 10 % range in either the vehicle or paclitaxel based arm of the screen. A cell viability ratio was then calculated as $mean_{paclitaxel}/mean_{vehicle}$ and used to calculate a z-score for each siRNA (Figure 4B and C). The z-score was calculated using the formula: $z\text{-score} = (z - \mu)/\sigma$ where z = the calculated cell viability ratio for an individual siRNA, μ is the average ratios for all siRNAs for each day of screening and σ is the standard deviation of all ratios for each day screening. To identify chemosensitizing siRNA, we were interested in those that had a ratio $z < -2.5$ and had at least a 15 % cell viability decrease in the presence of paclitaxel. As we are specifically interested in those siRNA that support deflection of mitotic stress induced death, we also eliminated those siRNA pools that caused a cell viability defect of 15 % or greater in the presence of vehicle alone from further consideration. Finally, to

enrich for those genes that may have a therapeutic window, siRNA pools that impacted cell viability in a normal bronchial epithelial immortalized cell line, the HBEC3KT's, were also removed from further analysis [74]. Ultimately, this analysis identified 49 candidate siRNA pools that correspond to annotated genes in the GENE database (Table 1). Depletion of the identified candidate chemosensitizers has minimal impact on cell viability on their own, but decreases cell viability by at least 15 % in the presence of sublethal dose of paclitaxel.

The identified chemosensitizers impact many diverse pathways, illustrating the global effect a drug or perturbagen can have on a cell system (Figure 4D and Table 1). The high interest chemosensitizers include a wide variety of proteins shown to regulate transcription. We identified MTPN, which regulates NF-kappa-B signaling [75], and SATB1, which is a transcriptional repressor that functions as a chromatin-remodeling factor and has been implicated in several tumorigenic settings [76-78]. Several genes that modify post translational modifications were also identified, including phosphatases, phosphatase inhibitors and components of the ubiquitin ligase cascade. These genes likely serve as nodes critical to regulating paclitaxel resistance. Further, we identified genes with more direct links to paclitaxel's mechanism of action. We identified tubulin-binding cofactor C (TBCC) and tubulin tyrosine ligase (TTL), which are proteins integral to tubulin protein folding and posttranslational modification, respectively [79, 80]. Further, there was a small cohort of genes that play a defined role in mitosis, such as ANAPC5, a critical component of the anaphase promoting complex, and CENPP, a mitotic centromere protein [81].

Interestingly, we also identified a large number of genes with unknown or

unannotated function and several ‘pseudogenes’. Pseudogenes have been considered junk, or non-functional DNA, for a long time; however, since the ability to perform genome wide RNAi functional screens has been developed, it has become increasingly apparent that these “junk” genes can be critical to regulating numerous processes [82]. They have been found to regulate tumor suppressors and oncogenes and can be deregulated in cancer. Here, we suggest that due to the broad network engaged in paclitaxel resistance, there are likely novel therapeutic entry points with which to push taxane therapeutic strategies forward.

Secondary screening analysis

In order to identify the genes and processes most integral to paclitaxel resistance, we chose 23 candidates from a broad range of biology for additional secondary analysis. These candidate chemosensitizers were assessed for their ability to induce apoptosis, as measured by activation of caspase-3 and -7, and also their impact on mitotic progression and fate (Figure 5A and B). To monitor the impact of gene depletion on mitosis, a small scale, live-cell imaging screen was performed in HCC366 cells engineered to express GFP-H2B. Cells depleted of candidate chemosensitizers were evaluated for the amount of time spent in mitosis from nuclear envelope breakdown to cytokinesis, and the resulting mitotic fate was monitored. Further, to validate that the candidate siRNA pools were in fact knocking down their intended gene, target mRNA levels were also assessed (Figure 5C).

This secondary screening analysis further stratified identified siRNAs into four categories (Figure 5D). Group I had little to no impact on mitotic progression or induction of apoptosis. Depletion of genes in group II caused a prolonged mitotic delay

but less than a two fold increase in caspase induction. Genes identified in group III increased cell death, however they did not significantly impact mitotic timing. Group IV had a significant increase in both mitotic timing and cell death. Depletion of group IV genes, in addition to increasing mitotic delay by at least 20 %, exhibited the greatest induction of apoptosis. Importantly, all four of group IV siRNA pools met our criteria for off-target validation by having at least two of the four independent siRNAs, or a second non-redundant pool, recapitulate the loss of cell viability phenotype of the screen (Figure 5E). The four identified group IV chemosensitizing genes are ANAPC5, a core scaffolding component of the APC [81], CASC1, which had previously been implicated in lung tumorigenesis [83], PDE3B, a phosphodiesterase that has been recently identified to sensitize lung cancer cells to cisplatin [84], and TRIM69 [85], an uncharacterized E3 ubiquitin ligase.

Prolonged engagement of the SAC recouples mitotic damage to cell death

Live-cell imaging was used to determine how cells depleted of cohort IV genes responded to paclitaxel at the single cell level. This analysis revealed that while depletion of this cohort produces a mitotic delay, all mitotic cells eventually aberrantly exited mitosis into a damaged micronucleated state (Figure 6A). Within the constraints of our imaging analysis, we were able to observe 40-50 % of the post-mitotic micronucleated cells undergo subsequent cell death as indicated by nuclear blebbing and loss of movement. The cell death observed at the single cell level is sufficient to induce a population viability defect as indicated by a minimum 50 % reduction in colony formation assays (Figure 6B). Finally, depletion of this cohort prolonged a paclitaxel-induced mitotic delay, as assessed by mitotic index, in three additional paclitaxel-

resistant cell lines (Figure 6C). Together, these data indicate that ANAPC5, CASC1, PDE3B and TRIM69 are components that contribute to mitotic slippage in multiple genetic backgrounds.

To determine if the prolonged mitotic delay is required for post-mitotic cell death, cohort IV genes were co-depleted with siMAD2 in the presence and absence of paclitaxel and assessed at both the single cell and population level. At the single cell level, co-depletion with siMAD2 rescued the paclitaxel-mediated mitotic delay and nuclear blebbing, indicative of decreased cell death (Figure 7A). Co-depletion also prevented accumulation of cleaved caspase-3 at the population level as assessed by western blot analysis (Figure 7B). Taken together, these data indicate that engagement of the SAC and prolonged mitotic arrest is necessary for this cohort to re-couple mitotic damage to cell death.

We next measured the impact of depletion of cohort IV genes on the accumulation of MCL-1. MCL-1 is an anti-apoptotic protein that has been reported to be slowly degraded during a prolonged mitosis [65, 66]. We found that depletion of CASC1 and TRIM69 resulted in reduced MCL-1 protein only in the presence of paclitaxel, suggesting that it is coupled to the prolonged mitotic delay. In contrast, depletion of PDE3B suppressed MCL-1 either in the absence or presence of paclitaxel. Depletion of PDE3B on its own induced minimal cleaved caspase-3 accumulation, which may be attributable to this observed loss of MCL-1. MCL-1 is reported to be targeted for degradation by several E3-ubiquitin ligases including HUWE1/Mule, FBXW7 and the APC/C [65, 66, 86]. FBXW7 and APC/C have been shown to act on MCL-1 during mitosis while HUWE1 has been reported to be primarily active during interphase.

Preliminary evidence suggests that co-depletion of HUWE1 and PDE3B rescues siPDE3B-induced cell death in the absence of paclitaxel (data not shown). This data suggests that PDE3B may target MCL-1 in a non-mitotic manner. Accordingly, depletion of ANAPC5, a core scaffolding component of the APC/C, stabilizes MCL-1. The accumulation of cleaved caspase-3 despite ANAPC5-mediated stabilization suggests that there are additional apoptotic signaling pathways engaged to couple mitotic slippage to cell death.

Based on these results, we hypothesize that mitotic slippage is a prominent pro-survival mechanism in NSCLC, despite the resulting damaged and micronucleated cells. Thus, targeting precocious mitotic exit either directly through core checkpoint proteins, or indirectly through proteins implicated herein, may be a viable therapeutic option.

To begin addressing this hypothesis, we first examined direct inhibition of mitotic exit by depleting various APC/C subunits in the presence and absence of paclitaxel. Depletion of different APC/C subunits results in a range of caspase induction, suggesting that APC/C activity may be ‘tunable’ in order to find a therapeutically tractable level of inhibition. (Figure 8A). Furthermore, although the APC/C is essential and present in all cells, we find that tumor cells are more sensitive to ANAPC5 depletion as compared to normal cells (Figure 8B). To begin addressing the potential pharmacological benefit of direct inhibition of mitotic exit in combination with paclitaxel, HCC366 cells were treated with a combination of paclitaxel and proTAME. proTAME prevents association of CDC20 with the APC/C, thus directly inhibiting mitotic exit without impacting microtubule dynamics [87]. Here we found that combining proTAME with paclitaxel enhances both mitotic arrest, as assessed by accumulation of phospho-histone H3B, and

cell death, above the use of either agent alone (Figure 8C). Thus, a collaborative interaction exists between APC/C inhibition and paclitaxel in an otherwise paclitaxel resistant setting.

Inhibiting mitotic slippage *in vivo* abrogates tumor growth

While ANAPC5 is a well documented component of the anaphase-promoting complex, CASC1, PDE3B and TRIM69 have no clearly defined roles in mitosis. Given PDE3B's monogenic defects, we were particularly interested in further characterization of CASC1 and TRIM69. We next asked if inhibition of mitotic slippage, through stable depletion of CASC1 and TRIM69, would impact tumor cell growth *in vivo*. HCC366 cells were stably depleted of either CASC1 or TRIM69 and injected into the flank of immune-compromised mice to establish a xenograft model. By three weeks post-injection, tumors stably depleted of CASC1 and TRIM69 began to exhibit attenuation of tumor growth as evaluated by caliper measurement (Figure 9A and B). In an additional study, in which tumors from all mice were harvested at the same time, we observed a significant decrease in tumor volume in the shCASC1 and shTRIM69 tumors (Figure 9C). These findings suggest that CASC1 and TRIM69 support tumor cell growth *in vivo*. The remainder of this project has focused on elaborating the contributions of CASC1 and TRIM69 to mitotic slippage.

Discussion. This unbiased, pan-genomic loss of function screen for paclitaxel chemosensitizers identified mitotic slippage as a dominant mechanism governing innate paclitaxel response. Groups I, II and III from the secondary screening analysis remain intriguing to the study of paclitaxel resistance. Microtubule targeted drugs are thought to be efficacious because cancer lines generally exhibit unrestrained proliferation. Group I

and II's minimal induction of apoptosis suggests that the cell viability defect measured in the initial screen is likely due to other defects. For example, the observed viability defect may be due to an impact on proliferation. Thus, future investigation into additional genes that were not selected for further study herein is warranted.

Comparing groups II and IV, we see an un-coupling of mitotic delay and cell death. Depletion of all members of group II exhibit increased mitotic timing, yet minimal activation of caspase-3/-7 and apoptosis. In contrast, group IV recouples a minimum 20 % increase in mitotic delay to cell death. This begs the question, why do chemoresistance cells survive following depletion of group II genes. There may be many technical reasons for the observed uncoupling of mitotic delay and cell death. The uncoupling could be due to off target effects, insufficient depletion, or possibly cell death from depletion of group II targets may have been outside of the timing of our assays. However, if this is an on target effect, a mechanistic understanding of how mitotic timing has become uncoupled from cell death would advance the study of mitotic slippage. It is possible that a delayed mitosis only becomes re-coupled to cell death through discreet mechanisms and specific types of mitotic damage.

Analysis of group IV genes, reveals a cohort of proteins that support mitotic slippage, and thus cell viability, in the presence of a damaging dose of paclitaxel. This study presents pharmacological evidence that directly targeting mitotic exit through the APC/C may collaborate with paclitaxel treatment. Further, our APC/C subunit studies suggest that APC/C activity may be 'tunable' and thus, a therapeutic window may exist for directly targeting mitotic exit. Finally, as exemplified by CASC1 and TRIM69, this screen and secondary screening analysis has revealed that indirect methods of targeting

mitotic slippage do exist. These findings suggest that tumor cells engage previously unappreciated mechanisms to rapidly exit mitosis and evade cell death. It is possible that exploitation of these indirect mechanisms may have a superior therapeutic window over directly targeting core mitotic exit machinery.

Figure 3.

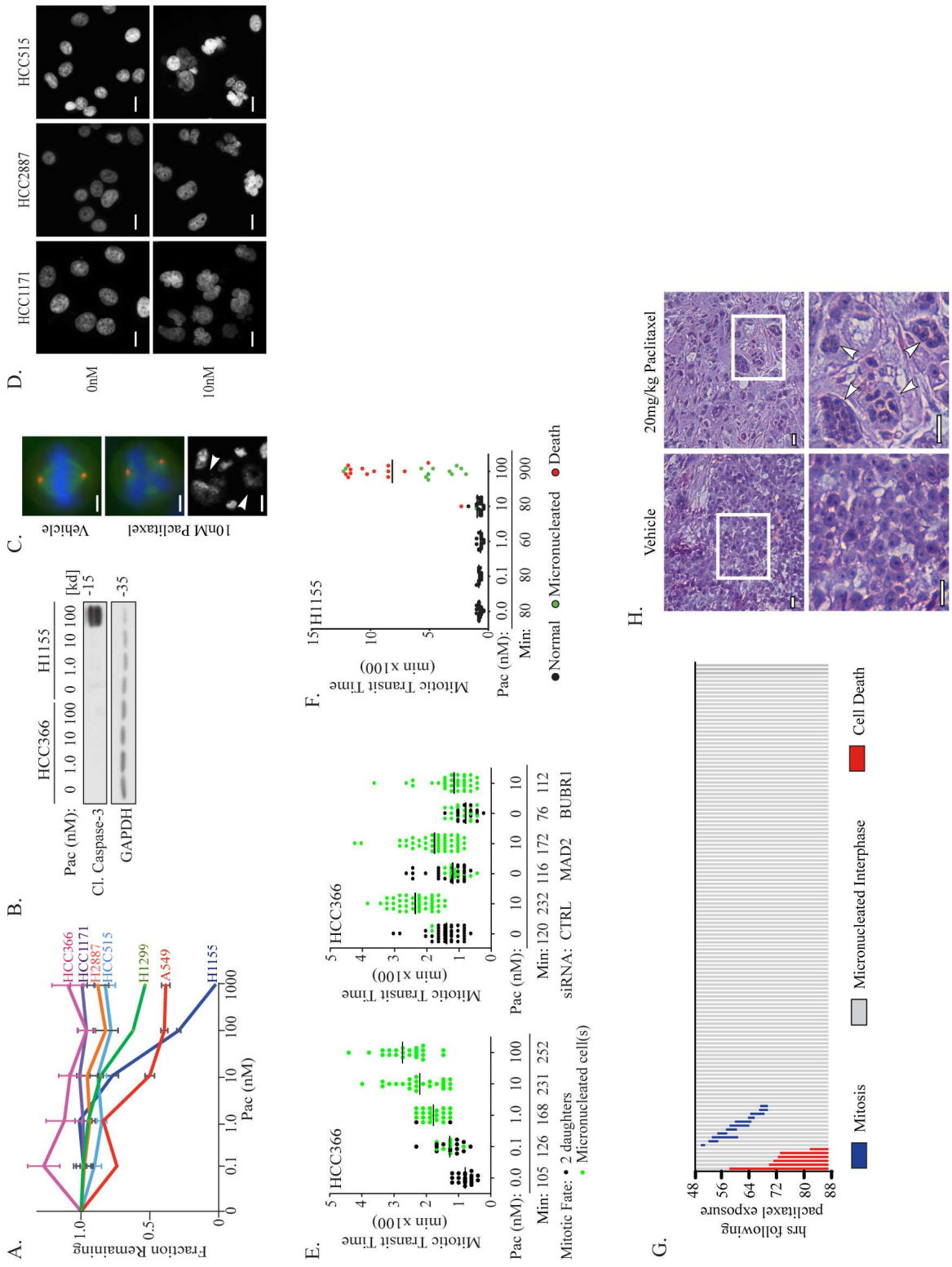
A.
Fraction Remaining
Pac (nM)
HCC366
HCC1171
H2887
HCC515
H1299
A549
H1155
B.
HCC366
H1155
Pac (nM): 0 1.0 10 100 0 1.0 10 100 [kd]
Cl. Caspase-3
GAPDH
-15
-35
C.
Vehicle
10nM Paclitaxel
D.
HCC1171
HCC2887
HCC515
0nM
10nM
E.
HCC366
Mitotic Transit Time (min x100)
Pac (nM): 0.0 0.1 1.0 10 100
Min: 105 126 168 231 252
Mitotic Fate: 2 daughters
Micronucleated cell(s)
Pac (nM): 0 10 0 10 0 10
Min: 120 232 116 172 76 112
siRNA: CTRL MAD2 BUBR1
F.
H1155
Mitotic Transit Time (min x100)
Pac (nM): 0.0 0.1 1.0 10 100
Min: 80 80 60 80 900
Normal
Micronucleated
Death
G.
hrs following paclitaxel exposure
Mitosis
Micronucleated Interphase
Cell Death
H.
Vehicle
20mg/kg Paclitaxel

Figure 3. Defining a paclitaxel-resistant NSCLC screening platform

(A) Indicated NSCLC cell lines were exposed to escalating doses of paclitaxel. Values represent the mean from a minimum of 3 independent experiments and error bars represent SEM. (B) HCC366 and H1155 cells were exposed to the indicated concentrations of paclitaxel for 48 hours and whole-cell lysates were immunoblotted with indicated antibodies. (C) HCC366 cells were exposed to paclitaxel for 24 hours followed by immunostaining for pericentrin (red), β-tubulin (green) and DAPI (blue, or grey in bottom panel). Arrows point to micronucleated cells. Scale bars represent 5 µm or 15 µm in bottom panel. (D) Indicated cell lines were exposed to paclitaxel for 24 hours and immunostained for DAPI. Scale bars represent 5µm. (E) Single-cell lineage tracing of HCC366 cells stably expressing GFP-H2B under indicated conditions. Each circle represents a single cell with the color of the circle representing mitotic fate. The bar indicates mean mitotic transit time of all cells under the specified condition. Left: Cells were exposed to the indicated doses of paclitaxel and imaged from 24 to 72 hours post drug exposure. 25 cells were evaluated for each condition. Right: Cells were transfected with indicated siRNAs and exposed to vehicle or paclitaxel 48 hours post transfection. Cells were imaged for 60 hours post vehicle or paclitaxel treatment. 50 cells were evaluated per condition. (F) Single cell lineage tracing of H1155 cells exposed to escalating concentrations of paclitaxel. 25 cells were evaluated per condition. Each circle represents a single cell with the color indicating fate of the mitotic cell. (G) Single-cell lineage tracing of HCC366 cells stably expressing GFP-H2B exposed to 10nM paclitaxel and imaged from 72 to 112 hours post drug exposure. 100 cells that were micronucleated at the start of imaging were evaluated. (H) H&E staining of HCC366 subcutaneous tumor xenografts treated with either vehicle or paclitaxel. Arrows indicate micronucleated cells. Scale bars represent 40 µm.

Figure 4.

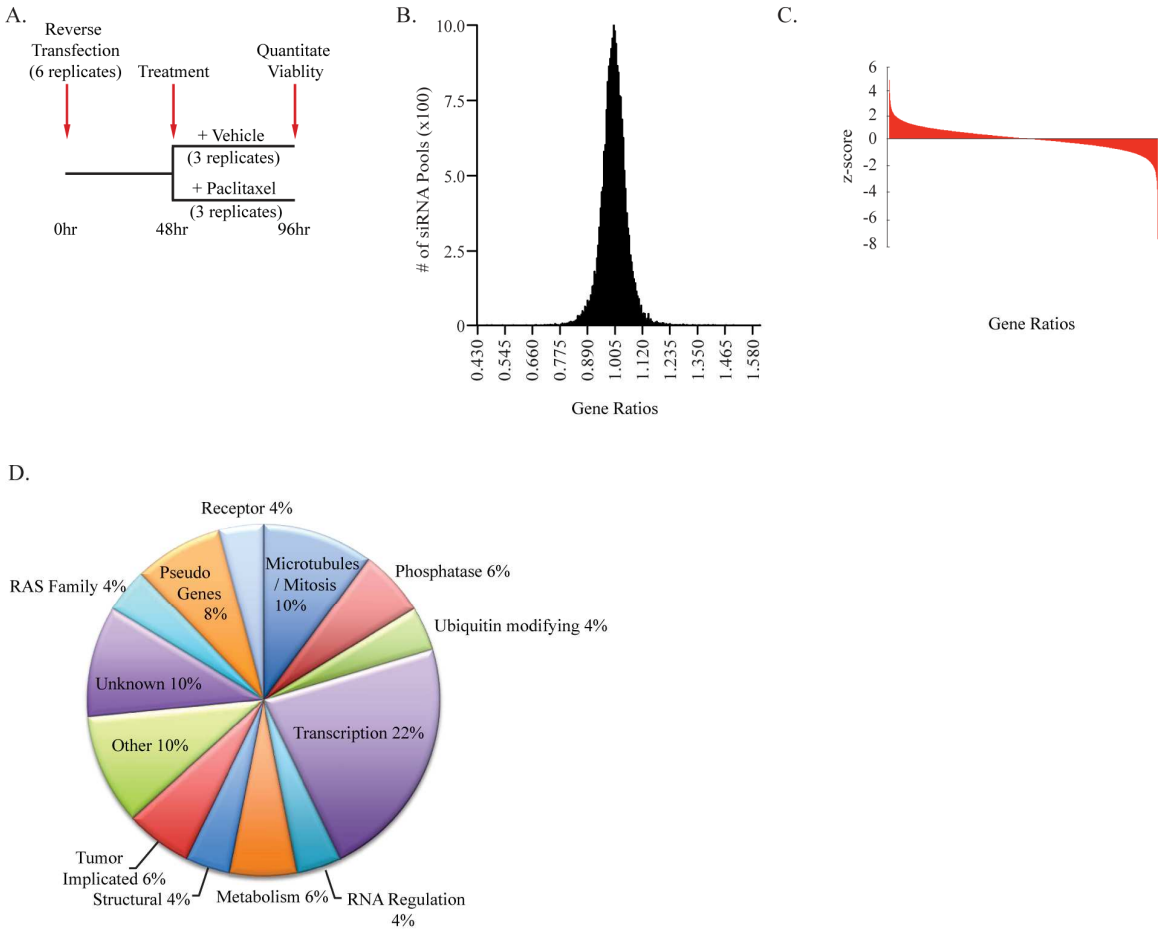

Figure 4. Pan-genomic loss of function screen in mitotic slippage prone HCC366 cells.

(A) Screening workflow for pan-genomic two-condition screen in HCC366 cells. (B). Histogram of cell viability ratios (treated/untreated). (C) Z-score distribution of ratios for each siRNA pool (D). Biological processes implicated by candidate chemosensitizers.

Table 1. High Interest Chemosensitizers

Table 1: High Interest Chemosensitizers

Symbol	Name	Symbol	Name
Microtubules/Mitosis		**Structural**	
ANAPC5*	anaphase promoting complex subunit 5	KRTAP3-1	keratin associated protein 3-1
BBS5*	bardet-biedl syndrome 5 protein	PLEC1	plectin
CENPP*	centromere protein P	**Tumor Implicated**	
TBCC*	tubulin folding cofactor C	TPD52*	tumor protein D52
TTL*	tubulin tyrosine ligase	CASC1*	cancer susceptibility candidate 1
Phosphatase		WWOX*	WW domain containing oxidoreductase
FIG4*	FIG4 homolog, SAC1 lipid phosphatase domain containing	**Other**	
LOC390760	protein phosphatase inhibitor 2-like	DNAJC22	DnaJ (Hsp40) homolog, subfamily C, member 22
MTMR9*	myotubularin related protein 9	PRDX3*	peroxiredoxin 3
Ubiquitin Modifying		SERPINB9*	serpin peptidase inhibitor, clade B (ovalbumin), member 9
FBXO21*	F-box protein 21	PDE3B*	phosphodiesterase 3B
TRIM69*	Ring Finger 36/ Tripartite Containing Protein 69	ATP8A1	ATPase
Transcription		**Unknown**	
FOSL1*	FOS-like antigen 1	C17orf100	chromosome 17 open reading frame 100
MTPN*	myotrophin	C9ORF173	hypothetical protein LOC441476
POLR2D	polymerase (RNA) II (DNA directed) polypeptide D	FLJ46026	FLJ46026 protein
POLR2G	polymerase (RNA) II (DNA directed) polypeptide G	MGC23918	coiled-coil domain containing 12
SATB1*	SATB homeobox 1	FLJ27354	uncharacterized LOC400761
TADA3L*	transcriptional adaptor 3 (NGG1 homolog	**RAS Family**	
TBX5	T-box 5	RAB3-GAP150	RAB3 GTPase activating protein subunit 2
TEAD3*	TEA domain family member 3	RAB6B	RAB6B
TLE4	transducin-like enhancer of split 4	**Pseudo**	
H1FOO	H1 histone family, member O, oocyte-specific	LOC201651	arylacetamide deacetylase (esterase) pseudogene
HLXB9	homeobox HB9; homeobox protein HB9; motor neuron and pancreas homeobox protein 1	LOC285412	TOX high mobility group box family member 4 pseudogene
RNA Regulation		SDHAP1	succinate dehydrogenase complex, subunit A, flavoprotein pseudogene 1
OAS3	2'-5'-oligoadenylate synthetase 3	LOC285697	TAF11 RNA polymerase II, TATA box binding protein (TBP)-associated factor, 28kDa
RBM22*	RNA binding motif protein 22	**Receptor**	
Metabolism		LOC285513/GPRIN3	G protein-regulated inducer of neurite outgrowth 3
PMM2	phosphomannomutase 2	TPRA40	transmembrane protein, adipocyte asscociated 1
YDJC*	YdjC homolog (bacterial)		
HADHA*	hydroxyacyl-CoA dehydrogenase/3-ketoacyl-CoA thiolase/enoyl-CoA hydratase (trifunctional protein), alpha		

* Denotes siRNA pools retested in secondary assays

Figure 5.

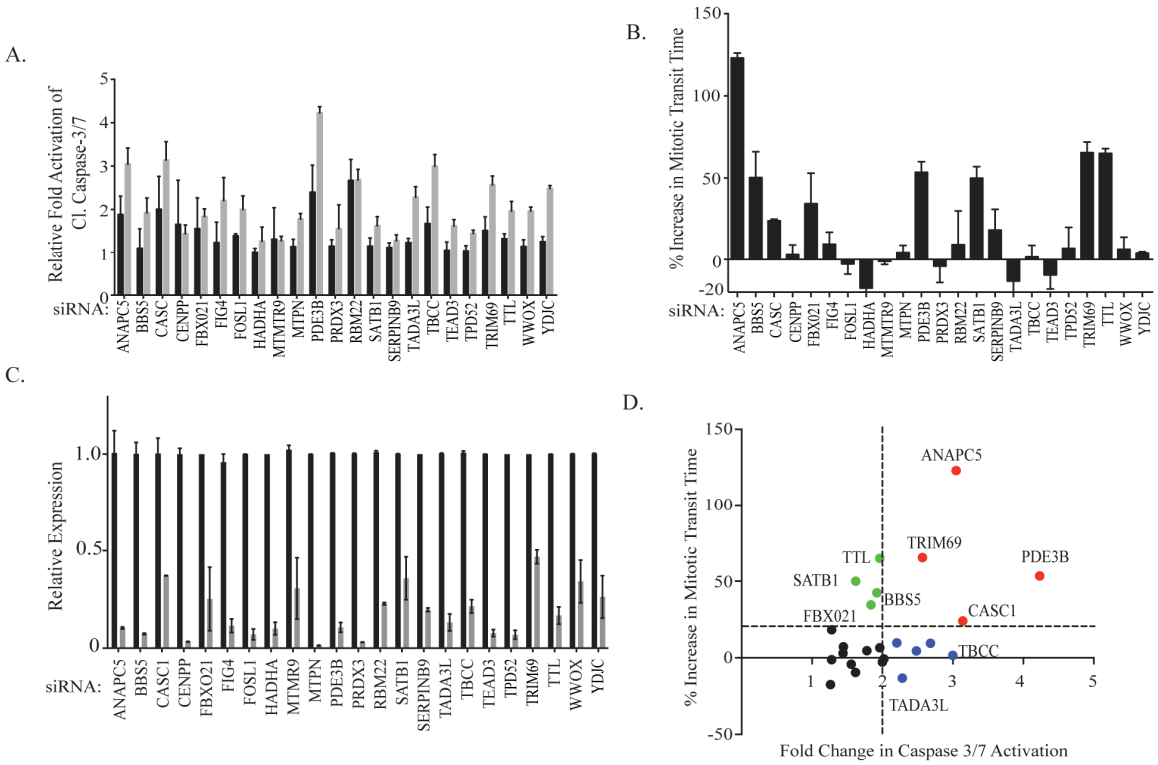

Figure 5. Secondary screening analysis stratifies candidate chemosensitizers

(A) HCC366 cells were transfected with indicated siRNAs for 48 hours. Cells were then exposed to vehicle (black bar) or 10 nM paclitaxel (grey bar) for an additional 48 hours. Cleaved-caspase 3/7 activity was assessed by APO-ONE. Values were normalized to control transfected cells under the same treatment (vehicle or paclitaxel) condition. Bars represent the average relative cleaved-caspase 3/7 activity over two experiments. Error bars represent range. (B) Lineage tracing of HCC366 GFP-H2B cells transfected with indicated siRNAs for 48 hours followed by exposure to 10 nM paclitaxel for 48 hours. Imaging commences following paclitaxel exposure. Bars represent the % change in transit time as compared to control transfected cells exposed to 10 nM paclitaxel from 2 independent experiments, which counted at least 50 cells each (30 cells for RBM22). Error bars represent range. (C) HCC366 cells were transfected with indicated siRNAs. 72 hours following transfection, RNA was harvested and target mRNA levels assessed by qPCR. Bars represent the average from 2 independent transfections. Error bars represent range. (D) Graph of secondary screening results. The y-axis represents the % increase of mitotic transit time as compared to control-transfected cells exposed to 10 nM paclitaxel. The x-axis represents caspase-3/7 activity relative to control values at the same dose. Group I – black, Group II – Green, Group III – blue, Group IV – Red.

Figure 6.

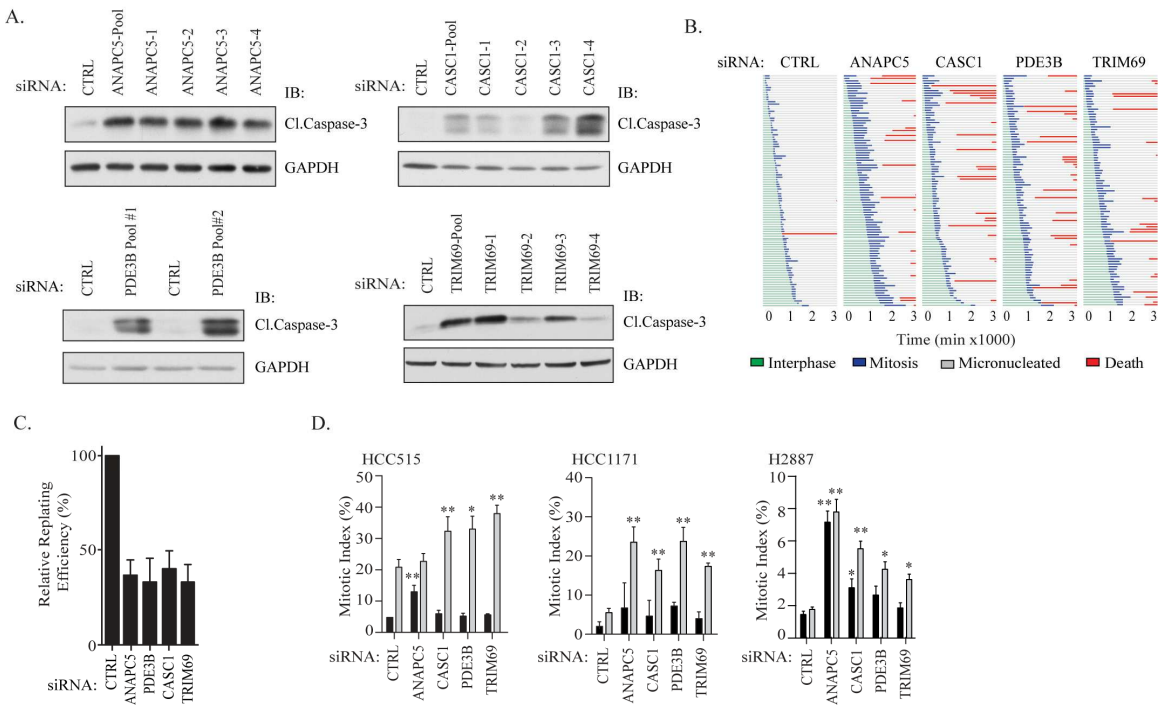

Figure 6. Pan-genomic screen reveals conserved regulators of mitotic slippage.

(A) HCC366 cells were transfected with indicated siRNA pools and individual siRNAs for 48 hours followed by exposure to 10 nM paclitaxel for 48 hours. Whole cell lysates were immunoblotted with indicated antibodies. (B) Single-cell lineage tracing of HCC366 cells stably expressing GFP-H2B following transfection with indicated siRNAs and exposure to 10 nM paclitaxel 48 hours post transfection. Cells were imaged for 60 hours post-treatment. Graph represents 50 cells assessed from 2 independent experiments. (C) Colony formation assay in HCC366 cells. Error bars are SEM for a minimum of 3 independent experiments. (D) Chemoresistant NSCLC cells lines were transfected with indicated siRNAs for 48 hours before exposure to vehicle (black bar) or 10nM paclitaxel (gray bar) for an additional 24 hours. Cells were fixed and stained for DAPI and phospho-histone 3B (ser10). Mitotic index was scored manually. Bars represent the average from 3 independent experiments and error bars represent SEM. p-values calculated by unpaired students t-test. * indicates p-value < 0.05. ** indicates p-value < 0.01.

Figure 7.

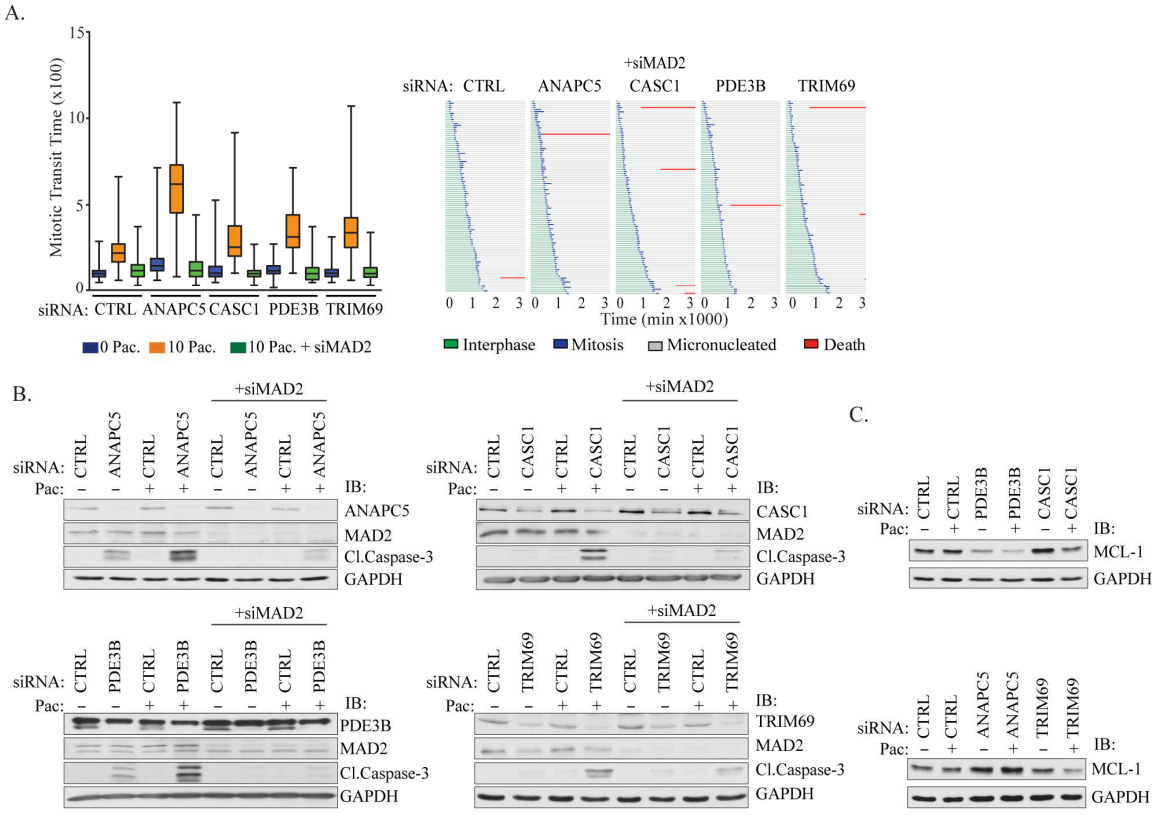

Figure 7. Prolonged engagament of the SAC recouples mitotic damage to cell death

(A) HCC366 GFP-H2B cells were co-depleted of siMAD2 in addition to indicated siRNA and monitored by live-cell imaging analysis as in figure 6 B. Left panel, box and whisker plot, bar represents mean mitotic transit time. Right panel, single cell lineage tracing. (B) HCC366 cells were transfected with indicated siRNAs for 48 hours before treatment with 10nM paclitaxel for an additional 48 hours as indicated. Whole cell lines were immunoblotted for indicated antibodies. (C) As in B.

Figure 8.

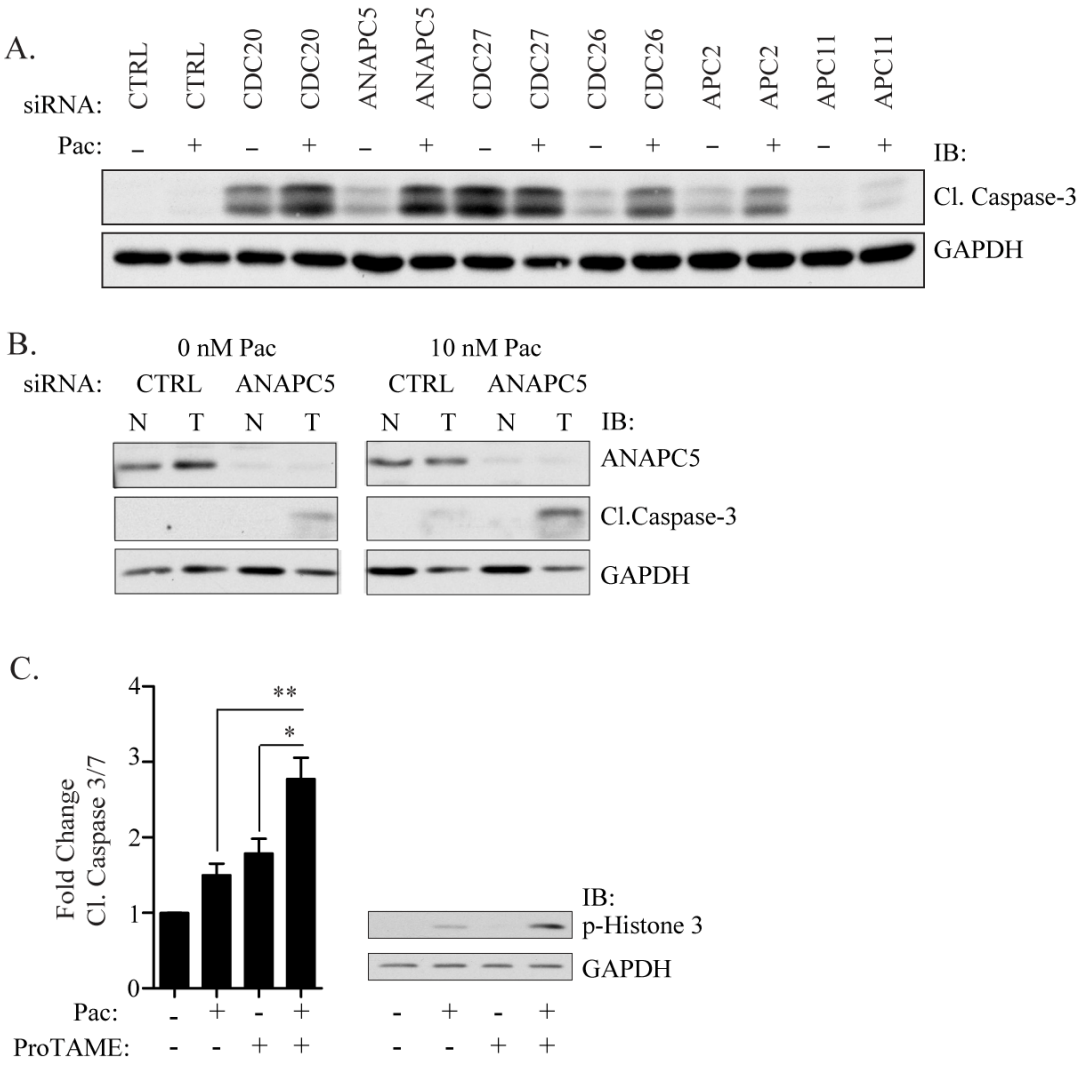

Figure 8. Direct targeting of the APC/C collaborates with paclitaxel treatment.

(A) HCC366 cells were transfected with indicated siRNAs for 48 hours before treatment with either vehicle of paclitaxel, as indicated, for an additional 48 hours. Whole cell lysates were immunoblotted for indicated antibodies. (B) Non-tumorigenic HBEC3KT (N) and NSCLC HCC366 (T) cell lines were transfected with indicated siRNAs for 48 hours and exposed to 10 nM paclitaxel as indicated for a subsequent 48 hours. Whole cell lysates were collected and immunoblotted for indicated antibodies. (C) Left panel: HCC366 cells were treated with vehicle, 10 nM paclitaxel, 2.5 µM ProTAME as indicated for 24 hours. Bars represent relative caspase 3/7 activity as assessed by APO-ONE® for 9 independent experiments. Error bars represent SEM. p values were calculated using a two-tailed unpaired student's t-test. * indicates p- value < 0.05. ** indicates p-value < 0.01. Right panel: HCC366 cells were treated with paclitaxel and ProTAME as in left panel. Whole cell lysates were immunoblotted with indicated antibodies.

Figure 9.

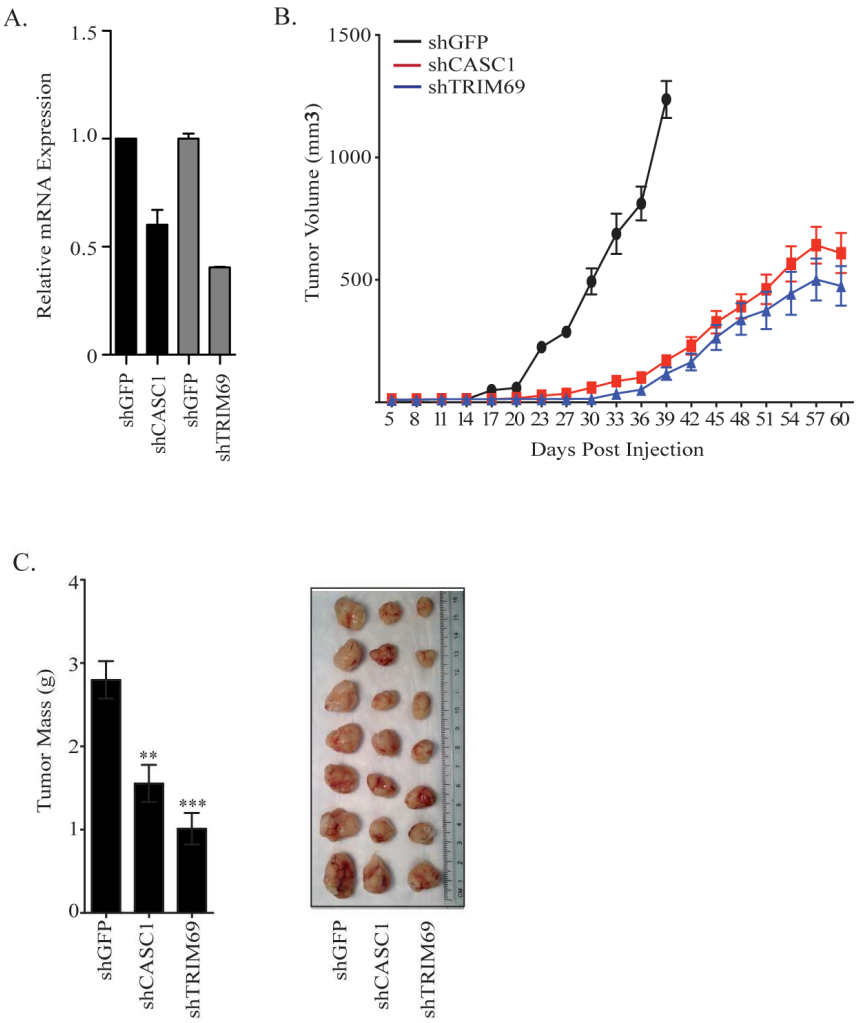

Figure 9. CASC1 and TRIM69 support tumor cell growth *in vivo.*

(A) mRNA expression levels of CASC1 and TRIM69 in HCC366 cells expressing indicated hairpins. Black bars represent CASC1 mRNA and grey bars represent TRIM69 mRNA. Error bars represent range. (B) Tumor growth curves for mice harboring HCC366 cells expressing indicates shRNAs. Each point represents n=9 (shGFP), n=9 (shCASC1) shCASC1 and n=7 (shTRIM69). (C) As in B except mice were sacrificed and tumors excised at 96 days post injections. Left panel: Average tumor mass. Error bar represent SEM; shGFP n=7 shCASC1 n=10 shTRIM69 n=8. p-value calculated by two-tailed unpaired t-test test. ** indicates a p-value <0.01. *** indicates a p-value < 0.0001. Right panel: Representative images of excised tumors.

Chapter IV. CASC1 regulates microtubule stability to support mitotic slippage

CASC1 Introduction:

Several lines of evidence suggest that there exists an inheritable genetic susceptibility to developing lung cancer [88-90]. To uncover these genetic predispositions free from environmental influence, Gariboldi et al took advantage of inbred mouse strains known to have varying degrees of susceptibility to urethane induced lung cancer, and performed a genome wide genetic linkage analysis [91, 92]. This analysis identified a region on mouse chromosome 6, later named the pulmonary susceptibility 1 (PAS1) locus, as responsible for approximately 50 % of the genetic variation between the two mouse models. Quantitative trait locus mapping by Zhang et al identified six candidate functional genes including the adjacent genes *Casc1* and *Kras* [83, 93]. *Casc1* has a single polymorphism at codon 60 resulting in a mutation from an aspargine to serine. This missense mutation is sufficient to alter tumor cell growth both by colony formation assays and in xenograft mouse models. While the mouse Casc1 and human CASC1 proteins are 67 % identical and 81 % similar, the key codon 60 is not conserved in the human homolog. Although there are no known genetic polymorphisms in human CASC1 that correlate with lung tumorigenesis or progression, ectopic expression of either mouse *Casc1* allele significantly limited tumor cell growth in the NSCLC A549 cell line [94].

CASC1 remains a largely uncharacterized protein with no known functional domains aside from a predicted coiled-coil domain in the amino-terminal. Further, a

search of publically available protein interaction databases reveals no known interactors. One report finds that the mouse Casc1 protein co-sediments and co-immunoprecipitates with β-tubulin [95]. Additional evidence shows that overexpression of Casc1 results in an accumulation of binucleated cells suggesting an aberrant mitosis [95]. Given this previous association with lung cancer, and beginning characterization data, identification of CASC1 as a potential chemosensitizer in paclitaxel resistant NSCLC suggests CASC1 may influence lung cancer biology.

Results

CASC1 supports cell viability and mitotic spindle integrity.

To begin to address the role of CASC1 in chemoresistance, CASC1 was depleted in a panel of NSCLC-derived cell lines of varying paclitaxel responsiveness. We found that CASC1 is essential for tumor cell viability either alone, or in the presence of paclitaxel in a number of NSCLC genetic backgrounds. However, we find no induction of caspase-3 in a normal immortalized human bronchial epithelial cell line the HBEC3KT cells (Figure 10A). On the single cell level, CASC1 depleted cells exhibit various mitotic defects both in the absence and presence of paclitaxel. In the H1299 cells, where CASC1 is required for cell viability, depletion results in increased accumulation of abnormal mitotic spindles, either multipolar or containing low tubulin density. Further, CASC1 depletion exacerbated the paclitaxel-induced mitotic spindle damage in the HCC366 cells (Figure 10B). The H1155 cells are considered a paclitaxel sensitive cell line which is less adept at undergoing mitotic slippage [68, 71]. H1155 cells stably expressing GFP-H2B were depleted of CASC1 and assessed by live cell imaging. Here we found that depletion had little impact on cell viability or mitosis on its own, but in combination with

paclitaxel, induced a dramatic mitotic delay which was frequently coupled to cell death in mitosis and aberrant mitotic figures. Together, these data suggest that CASC1 functions to buffer paclitaxel induced mitotic damage and support mitotic fidelity.

CASC1 stabilizes microtubule network.

Studies of the mouse homolog of CASC1 suggest an association with β-tubulin through a basic amino acid domain. This basic region is well conserved in the human protein suggesting that CASC1 may collaborate with paclitaxel treatment through a direct impact on microtubules [93, 95]. To date, no impact of CASC1 association with tubulin has been described.

To determine if CASC1 affects the microtubule cytoskeleton, we examined the microtubule network in H1299 cells where CASC1 impacts mitosis in the absence of paclitaxel. H1299 cells were depleted of CASC1 and assessed on the single cell level by immunofluorescence. This analysis revealed a diminished microtubule network in interphase (Figure 11A left). Differential centrifugation, which allows the separation of soluble and polymerized tubulin, confirmed that depletion of CASC1 results in a suppression of microtubule polymer formation (Figure 11A center). We also see a loss of acetylated tubulin, a general marker of microtubule stability, following CASC1 depletion (Figure 11A right).

To begin to assess how CASC1 may impact microtubule dynamics, we performed a microtubule regrowth assay. In this assay the microtubule network is completely dismantled by treatment with a high dose of nocodazole. Following nocodazole treatment, the drug is washed out and timepoints are collected as the cells recover and repolymerize their microtubule network. In this setting we find that CASC1 depleted

cells have an impaired ability to regrow their microtubule network both in interphase (data not shown) and mitotic cells (Figure 11B). Together, these data suggests that CASC1 is a global regulator of microtubule stability.

To further investigate how CASC1's impact on microtubules may alter mitotic slippage, we examined BUBR1 positive kinetochores during mitosis. BUBR1 is a key sentinel protein monitoring microtubule-kinetochore attachment (Figure 1). Following CASC1 depletion, we find an increased number of BUBR1 positive foci in mitotic cells, indicating fewer microtubule-kinetochore attachments are being made (Figure 11C). Together, these data suggest that CASC1's impact on microtubule stability directly supports mitotic spindle formation.

CASC1 as an oncogenic dependency.

To further assess the tumor-selective dependency of CASC1, we took advantage of an oncogenic progression model based on the normal bronchial epithelial cell line HBEC3KT [96]. Parental HBEC3KT cells, HBEC3KT cells following stable inhibition of p53 (HBE3KT-p53) and successively stable expression of oncogeneic KRAS (HBEC3KT-p53/+KRAS) were assessed for microtubule impacts and cell viability following depletion of CASC1. While CASC1's impact on microtubule stability is maintained in the progression model, the apoptotic marker, cleaved PARP, only accumulated in the HBEC3KT-p53 and HBEC3KT-p53/+KRAS cell lines, suggesting that oncogenic alterations drive a dependency on CASC1 for cell viability (Figure 12A and B). In agreement with this hypothesis, we find that CASC1 is amplified in 15 %, 25 % and 7 % of lung, ovarian and breast tumors respectively. This amplification has a strong tendency to co-occur with KRAS as these genes are found adjacent on human

chromosome 12 (Figure 12C and D). It has previously been reported, in this progression model, that p53 alterations are sufficient to drive altered microtubule stability [97]. Together, these data suggest that CASC1's functional support of microtubule stability may be necessary to buffer oncogenic stress.

Finally, we find that depletion of CASC1 induces damage to cells sufficient to drive stabilization of p53. In the normal HBEC3KT and HBEC30 cells this accumulation of p53 is sufficient to induce p21, suggesting a resulting delay in cell cycle progression. While CASC1 depletion in the tumor cells tested is able to stabilize p53, these cells are unable to induce p21 (Figure 12E). These data suggest a mechanism by which normal cells may survive CASC1 depletion as opposed to those tumor cells with a defective p53 signaling cascade.

CASC1 Discussion

The work presented here identifies CASC1 as a candidate chemosensitizer. We show that CASC1 is required for cell viability in multiple genetic backgrounds of varying resistance to paclitaxel including sensitive cell lines. Thus, the mechanisms identified in this work can potentially benefit paclitaxel based therapy regardless of resistance status. Further, we find that CASC1 depletion has minimal impact on normal bronchial epithelial background, in the absence or presence of paclitaxel, but becomes a dependency following the addition of an oncogenic stress such as loss of p53 or overexpression of oncogenic KRAS. Recent reports suggest that mitosis is damaged in altered KRAS genetic backgrounds [98, 99] and several groups have demonstrated mitotic damage induced by additional oncogenic alterations [100-104]. Given CASC1's role in supporting mitotic fidelity and frequent amplification, we suggest that CASC1

functions to buffer mitotic defects induced by oncogenic changes.

Further, we find that depletion of CASC1 stabilizes p53 and induces p21 accumulation in normal but not tumorigenic backgrounds. The stabilization of p53 could be the result of several potential mechanisms. Several lines of evidence indicate that post mitotic failure, or an aberrant mitotic exit, cells may undergo a p53 and p21 dependent G1 arrest (Figure 2). This defect has been illustrated following treatment with paclitaxel [105-107]. As CASC1 supports mitotic spindle formation, it is possible that the accumulation of p53 is the result of a general, damaged mitotic exit. p53 has also been shown to accumulate in the nucleus post low dose paclitaxel treatment that interferes with microtubule dynamics [108]. Thus, it is possible that the p53 read out may be due to CASC1 interphase defects. Further, p53 accumulation could be due to CASC1-mediated genomic damage in the absence of paclitaxel.

Regardless, the accumulation of p21 in the normal bronchial epithelial backgrounds, and not the tumor cells, suggests that, normal cells may exit the cell cycle in response to CASC1 depletion, where as tumor cells with defective p53 signaling networks continue to proliferate. Thus, as the tumor cells continue to proliferate, they will be more susceptible to subsequent paclitaxel treatment then the normal cells that have exited the cell cycle. This hypothesis is supported by previous findings that the loss of normal p53 function can sensitize cells to paclitaxel [109]. This suggests a mechanism by which CASC1 is specifically required for cell viability following loss of p53 in the oncogenic progression model and suggests targeting CASC1 may have a therapeutic window.

Finally, we find that CASC1 functions to support mitotic slippage and

microtubule stability throughout the cell cycle. Several lines of evidence have demonstrated that treatment with drugs that allow some microtubule connections to be made allow mitotic cells to slip out of mitosis faster than those that completely inhibit the microtubule network. This concept can be exemplified by treatment with paclitaxel versus nocodazole, [110-112]. Depletion of CASC1 decreases microtubule stability and polymer, thus, during mitosis, would decrease the ability to form kinetochore-microtubule connections. Accordingly, siCASC1 mediated loss of polymerized microtubules increases BUBR1 at the kinetochores during mitosis. Recent evidence suggests that the number of unattached kinetochores directly correlates to the rate of mitotic slippage [111, 113, 114]. Together, suggesting that CASC1 supports microtubule stability required to satisfy, or diminish SAC signaling during mitosis and allow rapid mitotic exit.

Figure 10.

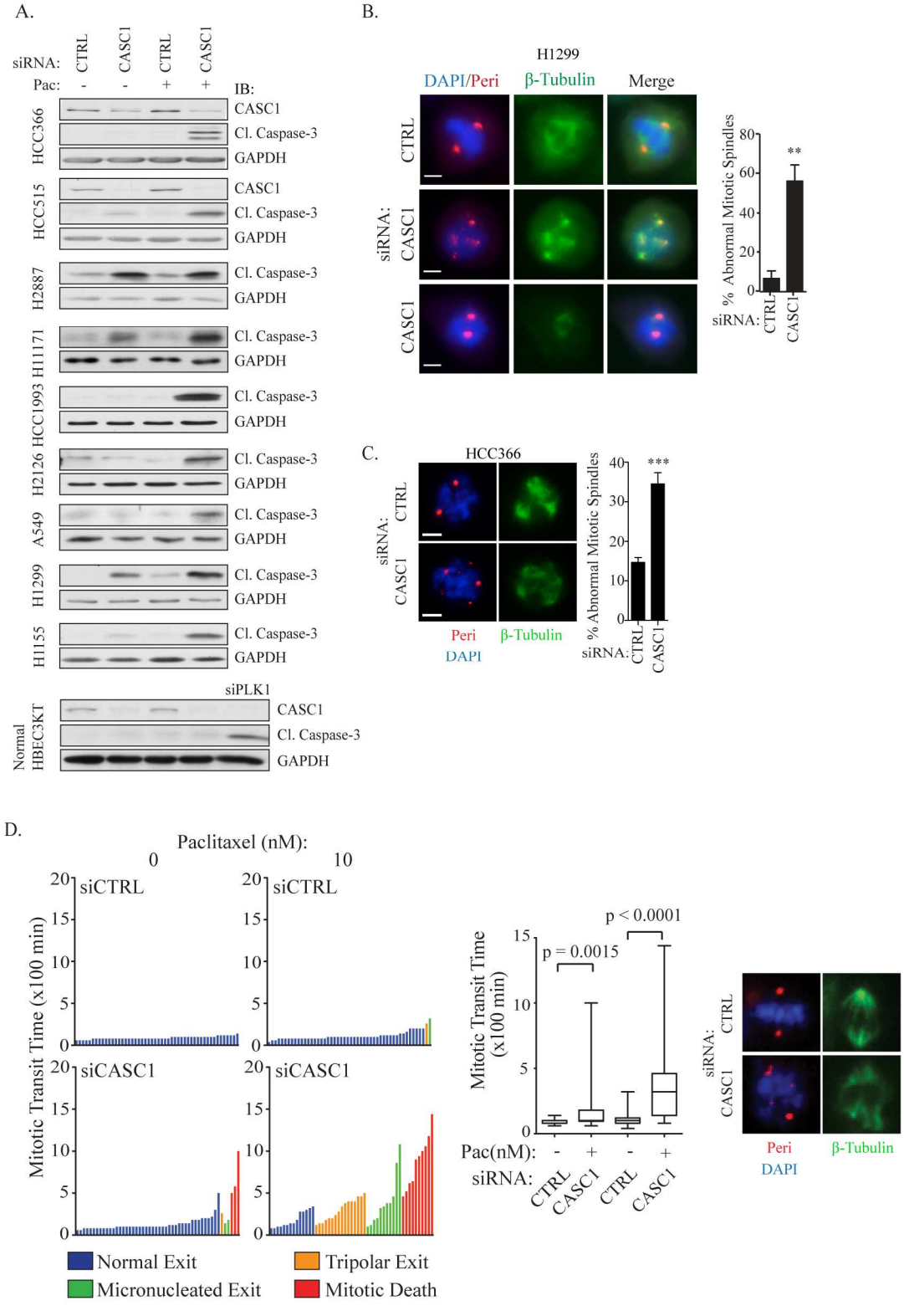
A.
siRNA:
Pac:
IB:
HCC366
HCC515
H2887
H11171
HCC1993
H2126
A549
H1299
H1155
Normal HBEC3KT
CASC1
Cl. Caspase-3
GAPDH
siPLK1
B.
H1299
DAPI/Peri
β-Tubulin
Merge
% Abnormal Mitotic Spindles
C.
HCC366
Peri
DAPI
D.
Paclitaxel (nM):
siCTRL
siCASC1
Mitotic Transit Time (x100 min)
Normal Exit
Tripolar Exit
Micronucleated Exit
Mitotic Death
p = 0.0015
p < 0.0001
Pac(nM):

Figure 10: CASC1 supports mitotic fidelity

(A) NSCLC cell lines were transfected with indicated siRNAs for 48 hours and treated with either vehicle or paclitaxel for an additional 48 hours. Whole cell lysates were immunoblotted with indicated antibodies. All cell lines were treated with 10 nM paclitaxel. siPLK1 was used as a positive control for cleaved caspase-3 in HBEC3KT panel. (B&C) Cells were transfected with indicated siRNAs for 48 hours then exposed to 10 nM paclitaxel for 24 hours. Subsequently, cells were fixed and immunostained with β-tubulin, pericentrin and DAPI. Scale bars are 5 μm. Abnormal spindles were manually scored as mitotic cells with <1 or > 2 pericentrin positive foci. Error bars represent SEM from a minimum of 3 independent experiments. p-values were calculated by two-tailed unpaired student's t-test. ** indicates a p-value < 0.01 and *** indicates p-value < 0.001. (D) H1155 cells stably expressing GFP-H2B were transfected with indicated siRNAs for 48 hours followed by exposure to 10 nM paclitaxel. Left panel: Single-cell lineage tracing was performed on 50 cells to measure length of mitotic transit time and mitotic outcome as previously described. Center panel: Box and Whisker plot of mitotic transit time is shown. *p* values were calculated with by Mann-Whitney test. Right panel: H1155s transfected and processed as in B&C.

Figure 11.

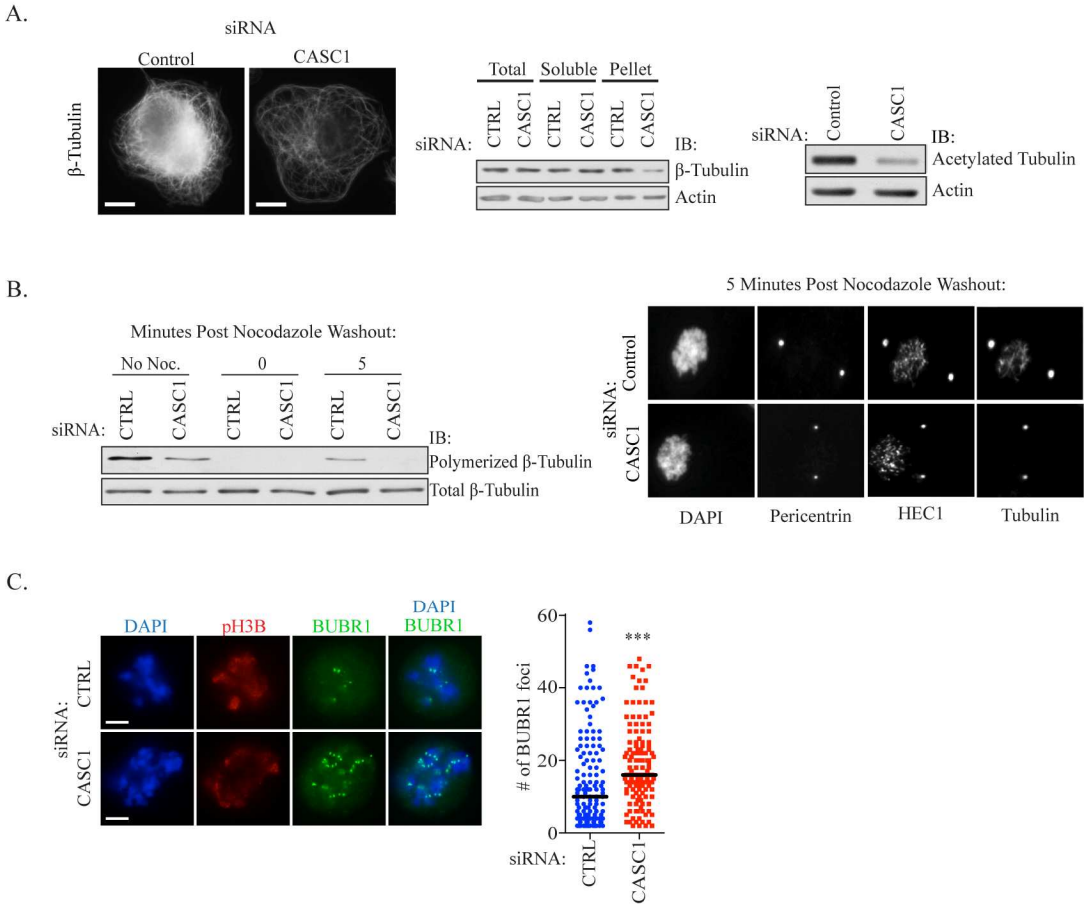

Figure 11: CASC1 supports microtubule stability to satisfy the SAC

(A) H1299 cells were assessed for CASC1 mediated impact on microtubules. Right panel: Cells were transfected as indicated for 72 hours followed by gluteraldehyde fixation and immunofluorescence processing. Center panel: H1299s were transfected as indicated and processed by an in vivo-polymerized tubulin assay. Right panel: H1299s were transfected and were immunoblotted as indicated. (E) Right panel: H1299s were transfected with indicated siRNAs for 72 hours. Cells were exposed to vehicle (no Noc.) or 11 μM nocodazole for 1 hour, followed by replacement with nocodazole-free medium for indicated times followed by an *in vivo* tubulin assay. Lysates were immunoblotted with indicated antibodies. Left panel: Microtubule regrowth assay was performed and cells were processed by immunofluorescence. (G) HCC366 cells were transfected as indicated for 72 hours.

Figure 12.

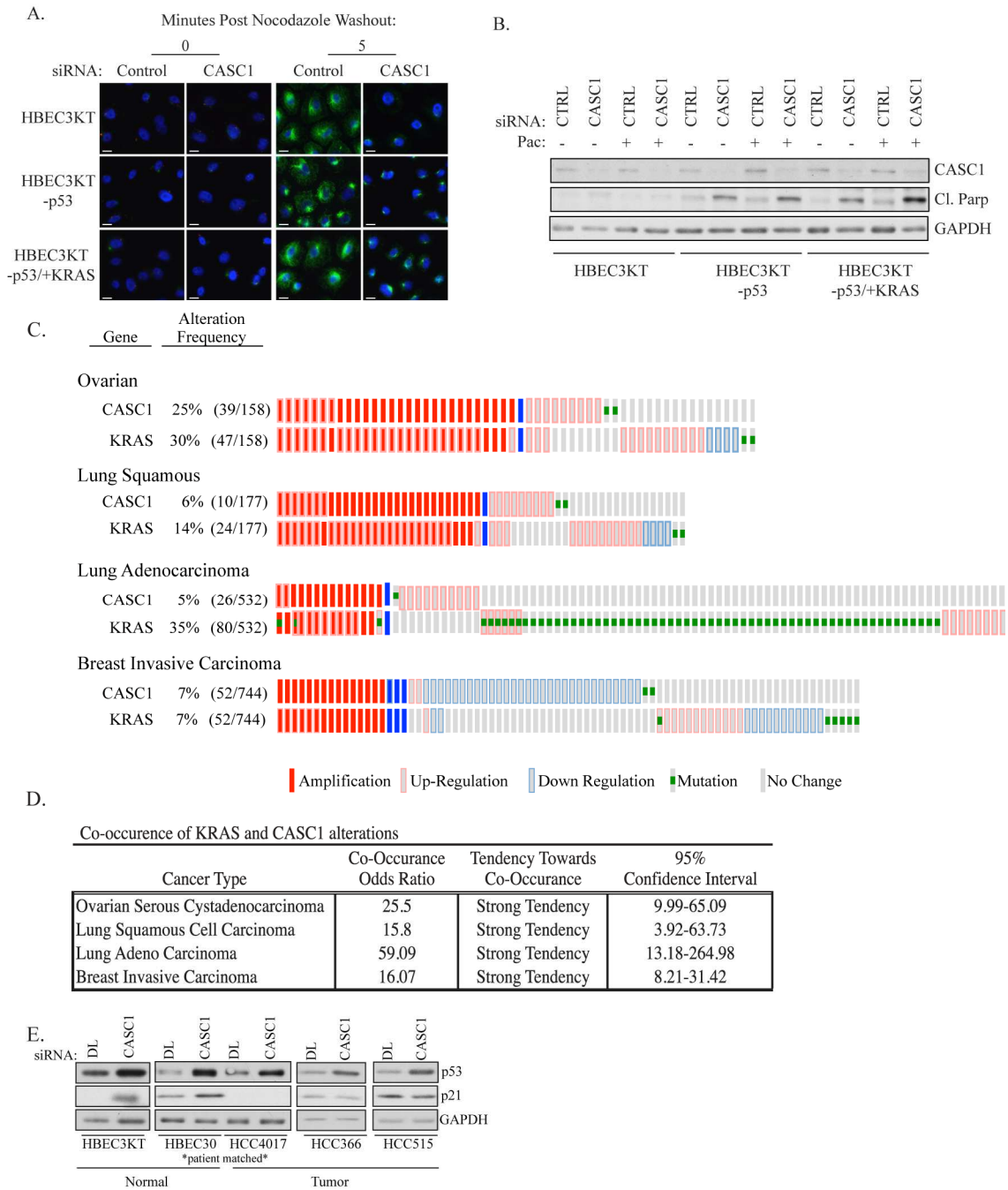

Cancer Type	Co-Occurance Odds Ratio	Tendency Towards Co-Occurance	95% Confidence Interval
Ovarian Serous Cystadenocarcinoma	25.5	Strong Tendency	9.99-65.09
Lung Squamous Cell Carcinoma	15.8	Strong Tendency	3.92-63.73
Lung Adeno Carcinoma	59.09	Strong Tendency	13.18-264.98
Breast Invasive Carcinoma	16.07	Strong Tendency	8.21-31.42

Figure 12. CASC1 is a tumor cell dependency

(A) Indicated cell lines were transfected with siRNAs for 72 hours before being processed by a microtubule regrowth assay and assessed by immunofluorescence. Red = pericentrin, Blue = DAPI, Green = β-tubulin. (B) Cell lines were transfected with indicated siRNAs for 48 hours followed by treatment with vehicle or 10nM paclitaxel for an additional 48 hours. Whole cell lysates were collected and immunoblotted for indicated antibodies. (C&D) Expression, amplification and co-occurance odds of CASC1 and KRAS in indicated tumor types. Data collected from publically available cBioPortal for Cancer Genomics hosted by Memorial Sloan-Kettering Cancer Center. (E) Cell lines were transfected as indicated for 96 hours. Whole cell lysates were collected and immunoblotted with indicated antibodies.

Chapter V. TRIM69 is a centrosomal and microtubule associated protein that is essential for mitotic fidelity.

TRIM69 Introduction:

TRIM proteins as E3 ubiquitin ligases. TRIM69 is a member of the TRIpartite Motif containing (TRIM) family of proteins characterized by an ensemble of three types of domains, a RING E3 ligase domain, one or two B box domains and a coiled-coiled domain [115, 116]. This specific architecture, referred to as a RBCC domain structure, is highly conserved in combination, order, and spacing. If one domain is missing in a TRIM family member, the remaining domain structure is conserved. This suggests that TRIM proteins have evolved to carry out a specific basic function common to all TRIM family members [117]. RING finger domains are primarily associated with E3 ubiquitin ligase activity, and while the presence of a RING domain does not dictate ubiquitin ligase function, the TRIM family has been broadly classified as a group of "single protein RING finger E3 ubiquitin ligases" [117].

Ubiquitylation is a common post-translational modification broadly used to regulate cellular physiology. Ubiquitylation is used in eukaryotic cells to regulate protein stability as well as protein activity, subcellular localization and regulation of trafficking among additional processes. These differential signals are achieved through regulation of ubiquitin chain length and the lysine used to form the isopeptide bonds of the ubiquitin chain. For example degradative ubiquitin signaling is achieved through polyubiquitin chain conjugation specifically through ubiquitin lysine 48. Rapid ubiquitination and

subsequent degradation is essential in order to respond to cellular signals such as satisfaction of the spindle assembly checkpoint [118].

The ubiquitin cascade is a complex and highly regulated, multistep mechanism achieved through sequential action of three enzymes, the ubiquitin activating (E1), ubiquitin-conjugating (E2) and ubiquitin-ligating (E3) enzymes. First, in an ATP-dependent manner, an E1 forms a thiol-ester bond with a free ubiquitin protein. The ubiquitin is then transferred to an E2 conjugating enzyme that then associates with an E3 ligase to transfer ubiquitin to the final substrate. Specificity increases going down the ubiquitin cascade. While there are two isoforms of the E1 activating protein, there are 35-40 potential E2 conjugating proteins and greater than 600 putative E3 ligases. E3 ligases are broadly classified based on their mechanism of transferring the activated ubiquitin from the E2 to the substrate. The primary E3 ligases families are the HECT (Homologous to E6Ap carboxy terminus) domain E3's and the RING (really interesting new gene) finger-containing E3's [119].

The HECT family, consisting of about 30 members, transfers the activated E3 to the substrate through a catalytic intermediate where the ubiquitin associates directly with the E3. The RING domain family proteins do not form an intermediate with ubiquitin but instead function as a rigid scaffold to bring an E2 and substrate into close proximity [119]. The RING domain coordinates two zinc ions through a conserved sequence of cysteine and histidine residues to form a characteristic 'cross-brace' structure. It has previously been demonstrated that mutation of the conserved cysteines can prevent zinc coordination and appropriate RING domain mediated associations [119, 120]. Mutation of conserved cysteines of the RING domain is used in localization studies of TRIM69

performed herein. RING family proteins can function as E3 ligases as part of large complexes, such as the APC/C and SCF (Skp1-Cullin-F-Box), or as in the case of TRIM proteins, as single protein ubiquitin ligases [119, 120].

TRIM protein function in pathological conditions. The TRIM family contains over 70 known members which have been implicated in a broad range of biological processes including development, differentiation, apoptosis and cell proliferation. A number of TRIM family proteins have previously been implicated in cancer and other pathological diseases [115]. TRIM18, or MID1, associates with microtubules throughout the cell cycle and targets the catalytic subunit of protein phosphatase 2 (PP2) for degradation [121]. Mutation of TRIM18 in the genetic syndrome, X-linked Opitz syndrome, results in decreased affinity for microtubules and altered PP2 activity which have been linked to characteristic defects in midline body structures, such as eye spacing, defects in the trachea or esophagus and cleft palate [122].

TRIM proteins have been implicated in either positively or negatively regulating oncogenesis in a context dependent manner [115]. TRIM19 or PML is subject to a chromosomal translocation which results in a fusion protein with the retinoic acid receptor-α (RARα). This PML-RARα fusion specifically occurs in acute promyelocytic leukemia (APL) [123]. In addition, recent work has identified TRIM proteins as forming functional complexes with members of the melanoma antigen (MAGE) family of cancer-testis antigens [124].

Cancer-testis antigens (CTAs) are genes whose expression are typically restricted to the germline, but become aberrantly expressed in a wide variety of human tumors. CTAs are typically expressed in the immune-privileged testis, thus, their aberrant

expression in tumors was identified to illicit an immune response in cancer patients. Until recently, CTAs have largely been studied from the field of tumor immunology with the possibility of using CTAs as cancer vaccines to stimulate an anti-tumor immune response. However the functions of CTAs in tumorigenesis have gone largely unstudied [125]. If CTAs are identified to participate in specific molecular pathways, this would identify pathways engaged to support tumorigenesis. TRIM-MAGE associations are found to functionally enhance the basal activity of TRIM family proteins through a yet undefined mechanism [124]. For example, it was demonstrated that TRIM28, which is over expressed in gastric cancer, can associate with up to four MAGE family proteins which enhance TRIM28 mediated degradation of p53 [124]. Together, this demonstrates that TRIM family proteins can be usurped by cancer specific mechanisms to support tumorigenesis. As discussed below, we find that, like TRIM28, TRIM69 associates with MAGE family proteins.

TRIM69 is a testes enriched E3-ubiquitin ligase. TRIM69 was originally identified through a PCR screen of a mouse testis cDNA library in search of novel genes that regulate spermatogenesis. Shyu et al found that TRIM69 expression in the mouse is restricted to the germline, absent during embryogenesis and becomes expressed during the first round of spermatogenesis. This expression pattern suggests that TRIM69 may function in meiosis or later steps of spermatogenesis [126]. Accordingly we also find human TRIM69 expression enriched in, though not restricted to, the testis (Figure 13A). TRIM69 was identified as a member of the TRIM/RBCC family based on its conserved domain structure and amino terminal RING zinc finger (Figure 13B). There is protein evidence that two primary splice variants of TRIM69 are expressed with one, referred to

herein as TRIM69B, which does not contain the RING domain. While TRIM69's cellular function has not been elucidated, it has been shown to contain a functional RING E3 ubiquitin ligase domain which we and others have demonstrated is sufficient to induce autoubiquitylation (Figure 13C) [85]. Identification of TRIM69 as a candidate chemosensitizer, whose depletion had minimal viability defects on its own made TRIM69 an intriguing gene to further characterize.

Results:

TRIM69 supports mitotic fidelity. To begin to determine the genetic penetrance of TRIM69 in supporting chemoresistance, depletion was evaluated in a panel of NSCLC patient derived cell lines of varying sensitivity to paclitaxel. TRIM69 was found to be required for cell viability in the presence or absence of paclitaxel in all but one tumor line tested and further, there is no observed induction of apoptosis in the normal HBEC3KT cells (Figure 14A). In addition to TRIM69 depletion causing a delayed mitosis, we find an accumulation of micronucleated cells in A549 and H1299 cells in the absence and presence of paclitaxel respectively, and an enhancement of paclitaxel-mediated multipolar spindles in HCC366 cells (Figure 14B). Depletion of TRIM69 in HCC366 cells also increased the number of BUBR1 foci in mitotic cells, indicating that without TRIM69, fewer stable kinetochore-microtubule attachments are made (Figure 14C). These data support the hypothesis that TRIM69 functionally supports mitotic fidelity.

TRIM69 is a generally uncharacterized E3 ubiquitin ligase with two primary coding splice variants, -A which contains the amino terminal RING domain and the -B isoform that lacks the functional RING domain. To begin characterizing TRIM69, localization studies were performed through transient overexpression of TRIM69A,

TRIM69B and TRIM69A (C53S/C55S), a mutation of two conserved RING domain cysteines. TRIM69A was found to localize to microtubules in interphase and the spindle poles during mitosis. This localization is dependent, at least in part, on the RING domain as neither TRIM69B nor the RING domain mutant maintained microtubule or centrosomal accumulation (Figure 14D). TRIM69 association with microtubules induces microtubule bundling, a classic phenomenon observed with several microtubule associated proteins. The bundling resulting from overexpression of TRIM69A was sufficient to stabilize microtubules against nocodazole mediated depolymerization, indicating a more stable and likely crosslinked microtubule network (Figure 14E). Consistent with TRIM69A specifically impacting microtubule dynamics, exogenous expression of -A and not -B disrupts mitotic spindle formation and drives accumulation of micronucleated cells, indicating aberrant mitotic exit (Figure 14F). Finally, siRNAs targeting knockdown of only TRIM69A only, were assessed for their impact on mitotic progression. Depletion of TRIM69A, specifically, was sufficient to prolong a paclitaxel-mediated mitotic delay in both the HCC1171 and HCC366 cells (Figure 14G). Taken together, these data suggest that the ubiquitylation activity of TRIM69A supports mitotic fidelity and, like many integral mitotic proteins, either depletion or over expression can have detrimental impacts on mitosis.

Given the link between a functional E3 domain and TRIM69 function, we next stably expressed myc-TRIM69A in H1299 cells to further study its regulation. At lower, stable levels of expression, TRIM69A is generally dispersed throughout the cytoplasm in interphase with a few strands associating with microtubules (data not shown). We found that TRIM69A is does not localize to centrosomes until entry in mitosis. myc-TRIM69A

remains at the spindle poles through cytokinesis (Figure 15A). Consistent with the observed localization, immunoprecipitation of endogenous pericentrin, a centrosome scaffolding protein, pulls down myc-TRIM69A (Figure 15B). Treatment with nocodazole was sufficient to disrupt myc-TRIM69A accumulation at the centrosome, indicating a microtubule-dependent recruitment (data not shown). Taken together, these data suggest that TRIM69A is recruited to the microtubule organizing centers (MTOCs) to support appropriate mitotic spindle formation.

TRIM69's interaction network.

Although both depletion and overexpression of TRIM69A results in mitotic errors, no overt spindle defects were observed following TRIM69A depletion. The exacerbated defects in the HCC366 cells are difficult to separate from paclitaxel damage, and although we observe segregation defects in the A549 and H1299 cells, chromosomes appear to align appropriately on the metaphase plate. Therefore, we used publically available databases, Mitocheck and the Broad, to identify potential TRIM69 interacting proteins and begin to assign a function to TRIM69. In agreement with TRIM69A's observed localization, several potential interactors support the cytoskeleton network, are/or associate with core centrosomal proteins, or have been implicated directly in altering mitosis (Figure 15C). To begin placing TRIM69 within this interaction network, we depleted a cohort of candidate interactors from H1299 cells stably expressing myc-TRIM69A and assessed myc-TRIM69A accumulation to the spindle poles. This analysis revealed that activity of two candidate interactors, MYPT1 and GNAI3, is essential for recruitment or maintenance of myc-TRIM69A at the spindle poles (Figure 15D). GNAI3, a Gialpha subunit, has been identified to localize to the centrosomes and its depletion

results in cytokinesis defects while its over expression results in a prolonged mitotic delay [127]. MYPT1, myosine phosphatase targeting subunit 1, forms a holoenzyme with the catalytic protein phosphatase 1 (PP1) and functions to target PP1 to substrates. In mitotic cells, MYPT1/PP1 has been found to be a negative regulator of PLK1 activity. Further, PP1 is integral to checkpoint silencing and removal of BUBR1 from kinetochores [128-131]. These results indicate a functional connection between TRIM69 and key mitotic proteins. Taken together, these studies have identified TRIM69A as a novel centrosomal component required for mitotic fidelity.

TRIM69 protein stability is regulated by a CT-antigen.

TRIM E3 ubiquitin ligases have recently been identified to functionally associate with the melanoma antigen (MAGE) family proteins [124]. In addition to centrosomal and cytoskeleton related candidate interactors, TRIM69's putative interaction network also identified MAGEA4. MAGEA4 has been found to be frequently over expressed in NSCLC and in our panel of cell lines we find expression of MAGEA4 in both HCC366s and H1299s (data not shown) [132]. Further, communication with Dr. Ryan Potts at UTSW uncovered an *in vitro* association between TRIM69 and both MAGEA4 and MAGEA12 (Figure 16A). These *in vitro* associations can also be detected in intact cells 24 hours post co-overexpression (Figure 16B). In performing this analysis, we find that co-overexpression of MAGEA4 results in a loss of TRIM69 protein stability at 48 hours post co-overexpression, suggesting MAGEA4 may post-translationally regulate TRIM69 (Figure 16C). In support of this hypothesis, depletion of endogenous MAGEA4 in H1299 cells stably expressing myc-TRIM69A stabilizes myc-TRIM69A protein and enhances TRIM69A association to the microtubule network. The MAGEA4-mediated change in

TRIM69 protein accumulation, accordingly, stabilizes microtubules against nocodazole depolymerization, indicating that the protein stabilization is physiologically relevant (Figure 16D and E). Further, MAGEA4 depletion in both HCC366s and H1299s results in accumulation of mitotic cells. Taken together, these data suggests that TRIM69 stability and thus, localization may be regulated by an aberrantly expressed cancer-testis antigen. Further, these data suggest that aberrant expression of cancer testis antigens may functionally support tumor cell mitosis.

TRIM69 discussion

Through the work presented here, we have found that TRIM69 is recruited to the mitotic spindle poles during mitosis to support mitotic fidelity. Localization to centrosomes requires an intact RING finger domain and further, depletion of the isoform that contains the RING domain is sufficient to drive mitotic defects. Together, these data suggest that TRIM69's E3 ubiquitin ligase activity is required to maintain mitotic fidelity.

Ubiquitylation events independent of the APC/C have been found to play critical roles in spindle formation and checkpoint silencing. For example, BRCA1 localizes to the centrosome during mitosis and ubiquitylates gamma tubulin to regulate centrosome splitting [133]. Recently, ubiquitylation of polo like kinase 1 (PLK1) was found to mediate degradation independent removal of PLK1 from kinetochores to facilitate checkpoint silencing [134, 135]. These studies demonstrate that E3 ligases can impact mitotic progression in ways independent of the APC/C. Now we have identified TRIM69 as a novel functional E3 ubiquitin ligase that supports stable kinetochore-microtubule attachments.

TRIM69 recruitment to the centrosome at the beginning of mitosis coincides with centrosome maturation. Centrosomes, as the microtubule organizing centers of the cell, undergo a process termed maturation at the onset of mitosis in order to expand microtubule nucleating capacity necessary for proper mitotic spindle formation [136]. Maturation is a dynamic process in which microtubule scaffolding proteins such as pericentrin accumulate at the centrosome and increase recruitment of microtubule nucleating proteins such as gamma-tubulin [136, 137]. Increased accumulation of gamma tubulin results in a dramatic increase in microtubule nucleation and thus, additional regulatory proteins are required to anchor microtubule ends to the centrosomes [138, 139]. The centrosomal maturation process is regulated by series of protein kinases and phosphatases including, but not limited to, PLK1 and PP1. TRIM69s cell cycle dependent recruitment to the centrosome, its demonstrated ability to bundle microtubules, and association with PP1 regulatory protein MYPT1 suggests TRIM69 may be required to support microtubule activities at the MTOCs during centrosomal maturation.

Several candidate centrosomal associated proteins were evaluated following depletion of TRIM69 in an effort to uncover TRIM69s impact on mitotic spindle formation. Unfortunately, our candidate approach uncovered no frank centrosomal or spindle errors. We may have been limited due to our visual resolution or we may have not identified the correct candidate protein. While we have been unable to clarify TRIM69's role at the centrosome, as with many critical mitotic proteins, we find that toggling TRIM69 expression or activity can have damaging impacts on mitotic outcome. TRIM69 depletion delays mitotic slippage, induces chromosomal segregation errors and engages cell death signaling programs. MAGEA4 may illustrate one mechanism engaged

by tumors to alter TRIM69 expression and alter mitotic slippage. Further, we see that recruitment of TRIM69 to the spindle poles relies, at least in part, on the activity of MYPT1 and GNAI3.

MYPT1 is one of several targeting subunits of protein phosphatase 1 (PP1) [140]. During mitosis, MYPT1 directs PP1mediated dephosphorylation of key mitotic regulator PLK1 [131]. Further, PP1 has been shown to support mitotic checkpoint silencing [141]. The functional association between TRIM69 and MYPT1 suggests possible mechanisms by which TRIM69 may impact mitotic slippage and thus, warrants continued investigation into the TRIM69 association with PP1.

Figure 13.

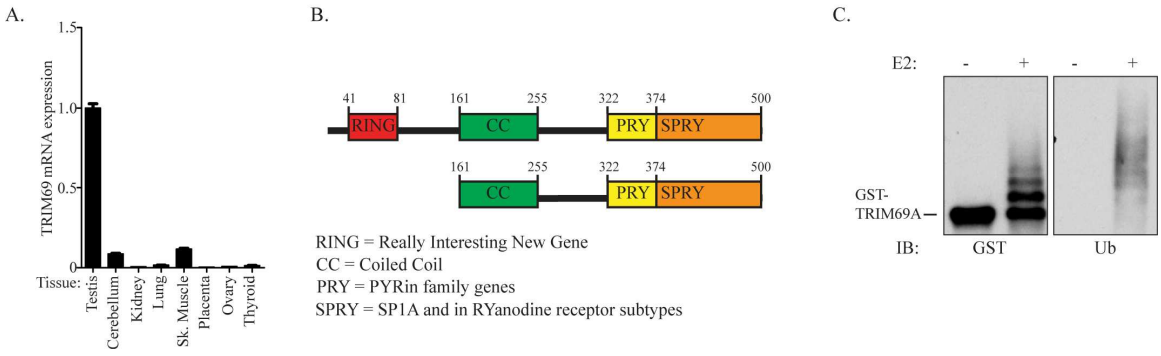

Figure 13. TRIM69A is a testes enriched E3 ubiquitin ligase.

(A) Commercially prepared RNA from human tissue samples were assessed for TRIM69 mRNA expression by qRT-PCR. (B) Domain structure of TRIM69. (C) *In vitro* auto ubiquitylation assay with purified TRIM69 in the presence and absence of the E2 enzyme.

Figure 14.

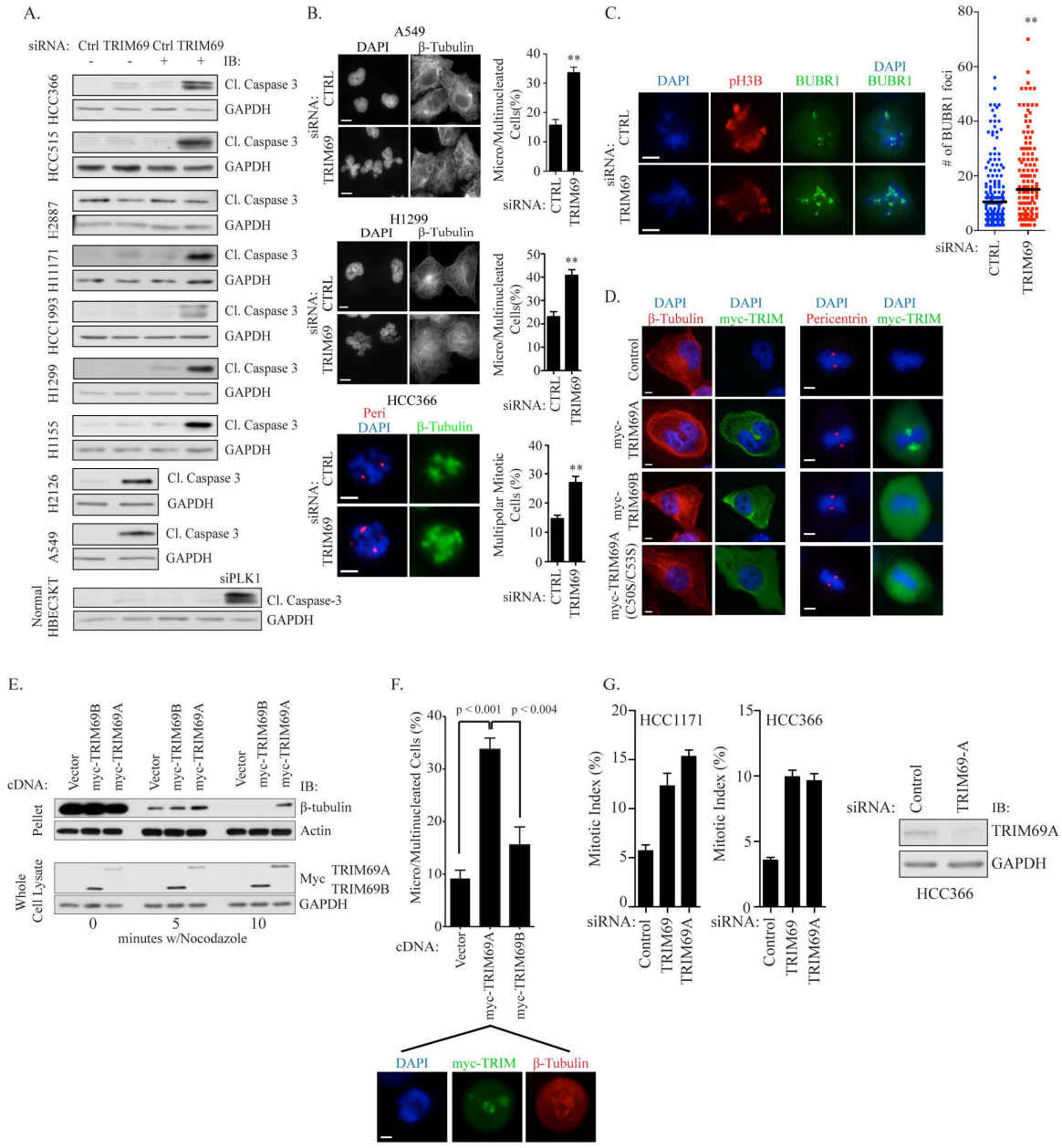
A.
siRNA: Ctrl TRIM69 Ctrl TRIM69
IB:
HCC366
HCC515
H2887
H11171
HCC1993
H1299
H1155
H2126
A549
Normal HBEC3KT
Cl. Caspase 3
GAPDH
siPLK1
Cl. Caspase-3
B.
A549
H1299
HCC366
DAPI
β-Tubulin
Peri
siRNA: CTRL TRIM69
Micro/Multinucleated Cells(%)
Multipolar Mitotic Cells (%)
C.
DAPI pH3B BUBR1 DAPI BUBR1
# of BUBR1 foci
D.
DAPI β-Tubulin
DAPI myc-TRIM
DAPI Pericentrin
Control
myc-TRIM69A
myc-TRIM69B
myc-TRIM69A (C50S/C53S)
E.
cDNA: Vector myc-TRIM69B myc-TRIM69A
IB:
Pellet
β-tubulin
Actin
Whole Cell Lysate
Myc TRIM69A TRIM69B
GAPDH
minutes w/Nocodazole
F.
p < 0.001 p < 0.004
Micro/Multinucleated Cells (%)
G.
HCC1171
HCC366
Mitotic Index (%)
siRNA: Control TRIM69 TRIM69A
TRIM69-A
TRIM69A

Figure 14. TRIM69A supports mitotic fidelity

(A) Indicated cell lines were transfected with indicated siRNAs for 48 hours followed by exposure to vehicle or 10nM paclitaxel for 48 hours. Whole cell lysates were immunoblotted for indicated antibodies. (B) Indicated cell lines were transfected with siRNAs for 72 hours then fixed and stained with indicated antibodies. HCC366 and H1299 cells were exposed to paclitaxel for the last 24 hours of transfection. Scale bars represent 10 µm for A549 and H1299 and 5 µm for HCC366. ** indicates a p-value < 0.01 by two-tailed unpaired student's t-test. (C) HCC366 cells were transfected with indicated siRNAs for 72 hours and immunostained with BUBR1. Scale bar represents 5 µm. BUBR1 foci were counted by manual inspection. Each circle represents a single cell. A minimum of 50 mitotic cells were evaluated per experiment for 3 independent experiments. p value was calculated by Mann-Whitney t-test. ** indicates a p-value < 0.05. (D) H1299 cells were transfected with cDNAs encoding myc-TRIM69A, myc-TRIM69B, myc-TRIM69A (C50S, C53S) or a control vector encoding Tomato-H3B. 24 hours post-transfection, cells were fixed and immunostained with indicated antibodies. Scale bars represent 5µm. (E) *In vivo* polymerized tubulin assay performed on H1299 cells transfected with indicated cDNAs for 24 hours followed by exposure to 11 µM nocodazole for indicated times. (F) Cells transfected and stained as in D were manually scored for multi or micronucleation. Bars represent mean from 2 independent experiments and error bars represent range. (G) Left panel: Indicated cell lines were transfected with siRNAs for 48 hours followed by exposure to 10nM paclitaxel for an additional 24 hours. Cells were fixed and stained with anti-phospho-histone H3 (ser10) and DAPI. Mitotic index was scored by manual inspection. Bars represent mean from 2 independent experiments and error bars represent range. Right panel: HCC366 cells were transfected with indicated siRNAs for 72 hours. Whole cell lysates were immunoblotted for indicated antibodies.

Figure 15.

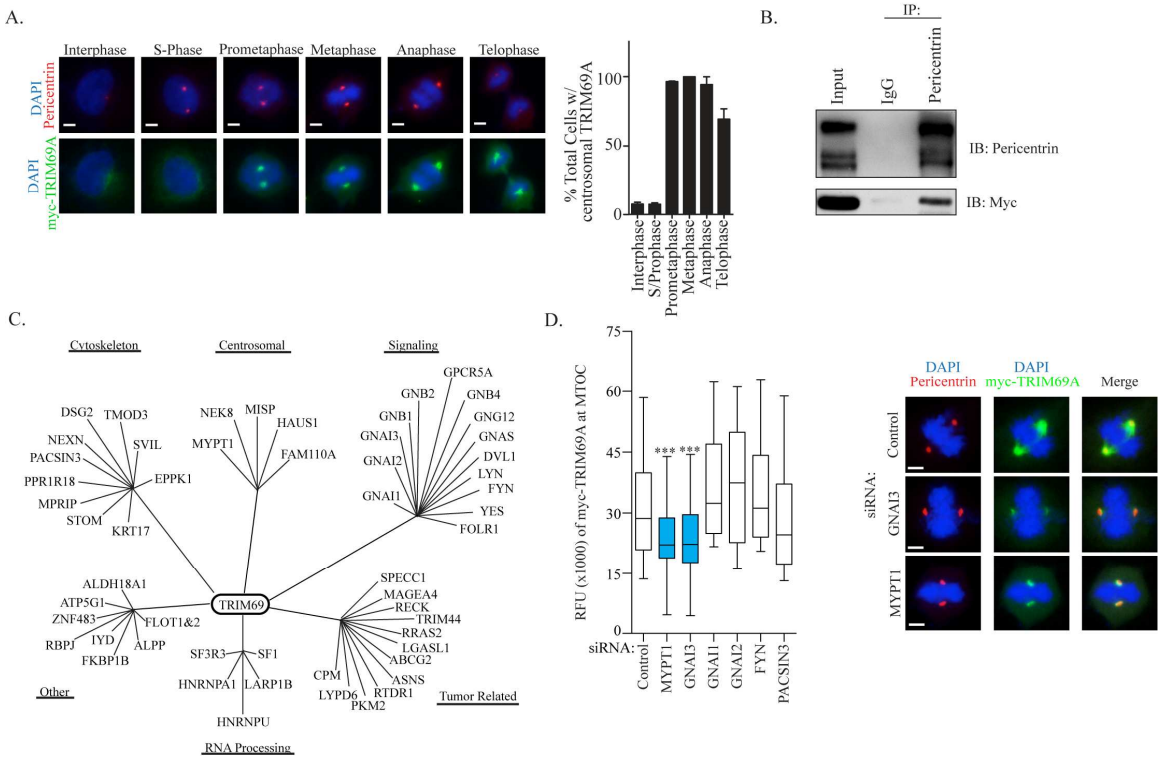

Figure 15. TRIM69A is a novel component of the MTOC

(A) H1299 cells expressing myc-TRIM69A were fixed and immunostained with pericentrin, myc and DAPI. Cells representing each stage in the cell cycle were identified based on nuclear morphology. Left panel: Representative images of cells during the cell cycle. Scale bar represents 5 µm. Right Panel: Quantitation of cells where myc co-localized with pericentrin as assessed by manual inspection. Bars represent the mean of 2 independent experiments and error bars represent range. A minimum of 100 mitotic cells was assessed per experiment. (B) H1299 cells stably expressing myc-TRIM69A were released from a double thymidine block for 3 hours followed by treatment with 100ng/mL nocodazole for 3 hours. Immunoprecipitation was performed using indicated antibodies. (C) Left panel: H1299 cells stably expressing myc-TRIM69A were transfected with indicated siRNA for 72 hours. Cells were fixed and stained for pericentrin, myc and DAPI. To quantify centrosome associated myc-TRIM69A, relative fluorescence of myc-TRIM69A at individual centrosomes (n>150 across 3 independent experiments) was measured with ImageJ and normalized for cytoplasmic fluorescence. Right panel: Representative images of mitotic cells transfected with indicated siRNAs.

Figure 16.

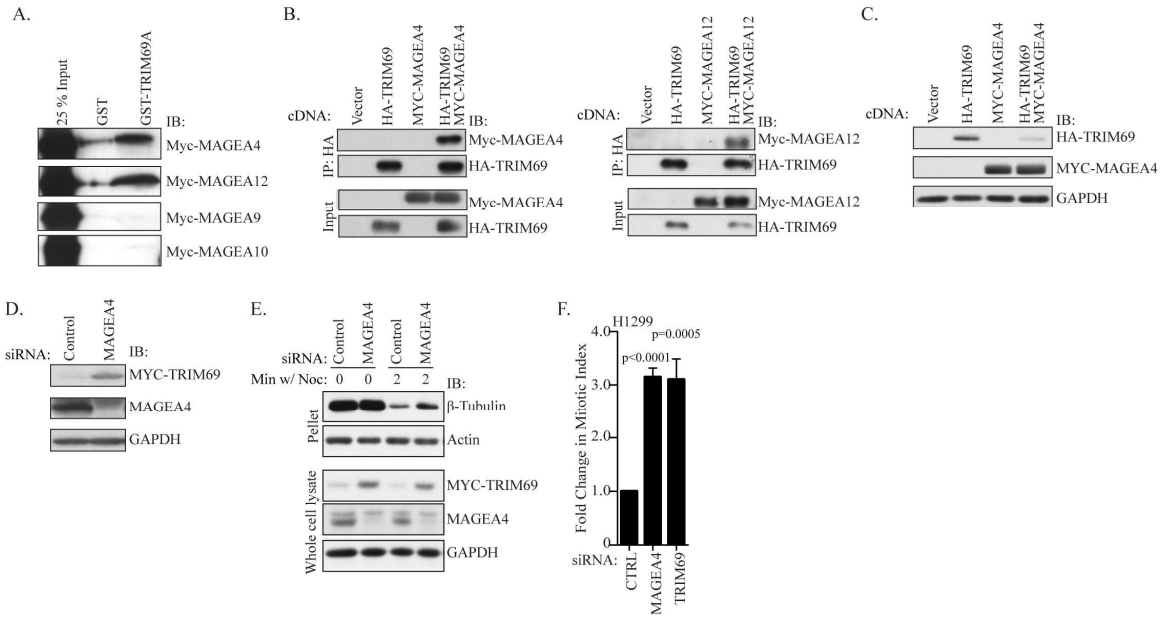

Figure 16. TRIM69 interacts with cancer testis antigen MAGEA4

(A) Immobilized GST- and GST-TRIM69A were incubated with indicated proteins. Samples were subjected to SDS-PAGE and immunoblotted with myc antibody. Contributed by Dr. Ryan Potts. (B) HEK293 cells were transfected with indicated constructs for 24 hours. Cells were lysed and immunoprecipitations were performed as indicated. Lysates and immunoprecipitates were immunoblotted with indicated antibodies. (C) HEK293 cells were transfected as in B, except lysates were taken at 48 hours. (D) H1299-mycTRIM69A cells were transfected with indicated siRNAs. 72 hours following transfection, whole cell lysates were immunoblotted with indicated antibodies. (E) H1299 myc-TRIM69 cells were transfected with indicated siRNAs for 48 hours then exposed to nocodazole for 0 or 2 minutes as indicated. Whole cell lysates were then immunoblotted with indicated antibodies. (F) H1299 and HCC366 cells were transfected with indicated siRNAs for 48 hours then exposed to 10 nM paclitaxel for 24 hours. Cells were subsequently fixed and immunostained with antibodies recognizing phospho-H3B and pericentrin and stained with DAPI. Mitotic Index was scored manually for 3 experiments. Error bars represent SEM. p values were calculated by unpaired student's t-test.

Chapter VI. Summary

Understanding the mechanisms that promote escape from mitotic-stress induced tumor cell death is vital to improving the current standard-of-care cytotoxic regimens for multiple cancers, including breast, ovarian and non-small cell lung cancer. The work presented here undertook a global analysis to identify mechanisms of intrinsic paclitaxel resistance. Importantly, in Chapter 3 we find that the most potent method of re-coupling mitotic stress to cell death is to prolong a paclitaxel-mediated mitotic delay. Further, we find that even in the most resistant genetic backgrounds, prolonging a mitotic delay by as little as 20 % can be sufficient to allow loss of pro-survival proteins and engage cell death signaling.

Mitotic slippage is observed in many tumor types and genetic backgrounds, suggesting it is a tumor survival mechanism despite the resulting genomic damage. Oncogenic perturbations, such as mutation of KRAS or loss of Rb, can have damaging impacts on mitosis. Thus, we hypothesize that tumor cells with mechanisms to rapidly exit mitosis, can bypass an oncogene induced mitotic delay and escape apoptosis. Those cells that can undergo mitotic slippage would have a selective advantage in tumor cell evolution and would inherently be more resistant to anti-mitotic drugs. If this hypothesis is correct, it is possible that the mitotic slippage prone cells would be more sensitive to an imposed mitotic delay. Indeed, we find that those mitotic slippage prone cell lines, such as the HCC366 cells, are much more sensitive to enforcing a mitotic arrest, through treatment with proTAME, then those cell lines known to tolerate a prolonged mitotic

delay, such as HeLa cells (Figure 17).

Identification of ANAPC5 as synthetic lethal with paclitaxel suggested that targeting the APC/C may have a therapeutic window. Previous studies have found that directly targeting mitotic exit, through depletion of CDC20, is highly lethal to cancer cells and "...killed all cells that entered mitosis.." [142]. Here, we were able to combine the APC/C inhibitor proTAME with paclitaxel and show a cooperative mitotic and cell death defect in the slippage prone HCC366 cells. We further expanded our analysis to additional APC/C subunits and found varying induction of cell death in the presence and absence of paclitaxel. Our studies suggest that APC/C inhibition may be 'tunable' in order to achieve a therapeutic effect.

In addition to directly targeting mitotic exit, we have identified novel mechanisms that indirectly support mitotic slippage. The work presented in chapter 4 identified CASC1 as a novel regulator of microtubule stability and suggested that separate but parallel insults to the microtubule network can collaborate therapeutically. Without CASC1, there is a loss of microtubule polymer that we propose leads to an insufficient ability to establish microtubule-kinetochore attachments. This defect ultimately leads to increased MCC protein BUBR1 at unattached kinetochores and an increased robustness of SAC signaling.

Several studies now describe an eventual satisfaction of the SAC, or a more rapid mitotic slippage, when cells retain some microtubule polymer [110, 111]. It is possible that mitotic slippage prone cells are more reliant on a stable microtubule network in order to rapidly silence the spindle assembly checkpoint. In further support of this idea, altering tubulin isoform expression to a higher ratio of βIII-tubulin, as is observed in many

models of paclitaxel resistance, decreases over all network dynamicity leading, generally, to a more stable network. Thus, we suggest that tumor cells with a more stable microtubule network may be more resistant to anti-mitotic therapy.

In chapter 5 we find TRIM69 to be a novel E3 ubiquitin ligase that localizes to the spindle poles in a cell cycle dependent manner. TRIM69 ubiquitylation activity is required for proper localization and mitotic fidelity. Though we have been unable to define the direct function of TRIM69 at the centrosomes, we do find that toggling TRIM69 expression can have damaging impacts on mitosis. Further, we find TRIM69 expression can be altered by a cancer-testis antigen, MAGEA4. These data suggest that re-expression of testis specific proteins can be functionally employed to buffer or support tumor mitoses. Further, we find a functional connection between TRIM69 and the centrosomal proteins MYPT1 and GNAI3. Over expression co-immunoprecipitation confirms that MYPT1 and TRIM69 can physically associate (data not shown). Given MYPT1s functional impact on PLK1 and association with PP1, one intriguing hypothesis is that TRIM69 may be regulating SAC silencing through impacting PP1 function.

Future Directions:

CASC1 depletion is found to have a global impact on microtubule dynamics both in mitosis and interphase. Altering the dynamics of interphase microtubules disrupts transport of several signaling pathways including Hif-1α [143], the androgen receptor [144], retinoblastoma (Rb) [145] and can result in an increase in p53 nuclear localization and transcription [146]. It is possible that the therapeutic benefit derived from treatment with paclitaxel may not be solely through impacting mitosis [147]. CASC1-mediated disruption of microtubule dynamics may have additional non-mitotic impacts that also

support cell viability in the oncogenic environment. Critical future work will focus on defining CASC1's interaction with tubulin, either with soluble heterodimers or with polymers. Defining which dynamic properties CASC1 alters and how it functions to support microtubule stability will further elucidate how CASC1 supports mitotic fidelity and tumor cell survival.

Similar to CASC1 having an impact on the cytoskeleton, examination of TRIM69's potential interaction network reveals a number of cytoskeleton related proteins. TRIM69 associates with MPRIP, which binds MYPT1 to facilitate integration of RhoA and ROCK signaling to the actin cytoskeleton [148]. TRIM69 also associates with phostensin (PPP1R18), which directs PP1 association with F-actin [149, 150]. Further, TRIM associates with nexillin (NEXN) an F-actin interacting protein that has been implicated in motility [151]. Given this actin axis in the TRIM69 potential interaction network, future studies may be directed at determining if TRIM69 impacts the actin cytoskeleton.

How TRIM69 functions at the centrosome to support mitotic fidelity remains an open question. Future studies will, first and foremost, be directed at elucidating TRIM69s role in mitosis. Investigation into potential interactors at the centrosome that have not been evaluated yet, such as HAUS1 and MISP, are of primary interest. HAUS1 is a component of complex that supports centrosomal and mitotic spindle integrity [152]. MISP is a newly annotated gene that is found to interact with the actin cytoskeleton and astral microtubules to regulate proper positioning of the mitotic spindle. Depletion of MISP results in a mitotic delay with increased BUBR1 positive kinetochores [153]. Thus, TRIM69's candidate interaction map reveals a wealth of potentially harvestable

information to help elucidate TRIM69's role in mitosis. This interaction map will be exploited as a starting point for defining TRIM69s mechanistic impact on mitosis.

In addition to elucidating TRIM69s interphase and centrosomal networks, future studies into the functional interaction between TRIM69 and the MAGE family CT antigens are warranted. We initially hypothesized that a functional interaction between MAGEA4 and TRIM69 may enhance TRIM basal ubiquitylation activity as observed with other TRIM-MAGE complexes [124]. While these studies with TRIM69 have not been fruitful to date, they were carried out in the absence of a known substrate. If TRIM69's mechanistic function at the centrosome or in interphase can be elucidated, evaluating MAGE proteins contribution to TRIM69's activity would be intriguing. Regardless of canonical TRIM-MAGE functional interaction, we have identified that depletion of both MAGEA4 and MAGEA12 (data not shown) results in an increase in mitotic index illustrating a delayed mitotic progression. This preliminary evidence suggests that tumor cells can engage testis specific mechanisms to support tumor cell mitosis, either directly, or through association with TRIM proteins.

Conclusion.

The work described here undertook a genome-wide loss-of-function screen in order to gain a mechanistic understanding of the uncoupling of mitotic damage from cell death. The primary finding from this study is that SAC signaling strength is tunable and can be altered to synergize with paclitaxel treatment. We have uncovered both direct and indirect molecular components that can alter SAC signaling, and in turn, APC/C activity, to collaborate with a sublethal dose of paclitaxel. Further, we have been able to illustrate this concept through both genetic depletion of our identified targets and pharmacological

inhibition of APC/C activity.

Finally, we posit that tumor cells evolve a reliance on mechanisms, such as CASC1 and TRIM69, in order to bypass mitotic-delay initiated death programs. In this manner, those tumors that harbor oncogenic changes that inflict collateral damage to mitosis, can survive, despite resulting genomic damage. This may be one reason for the widespread aneuploidy observed in patient tumors.

While some genetic alterations found in NSCLC patients are tractable for targeted therapy, a majority of patients continue to receive the paclitaxel based cytotoxic therapy. Unfortunately, the potential benefit of the standard of care regimen has not been achieved for NSCLC. The work described here identifies molecular components that could collaborate with paclitaxel treatment either to induce a response in resistant patients, or to lower the necessary therapeutic paclitaxel dose in responsive patients, to achieve better clinical outcomes.

Figure 17.

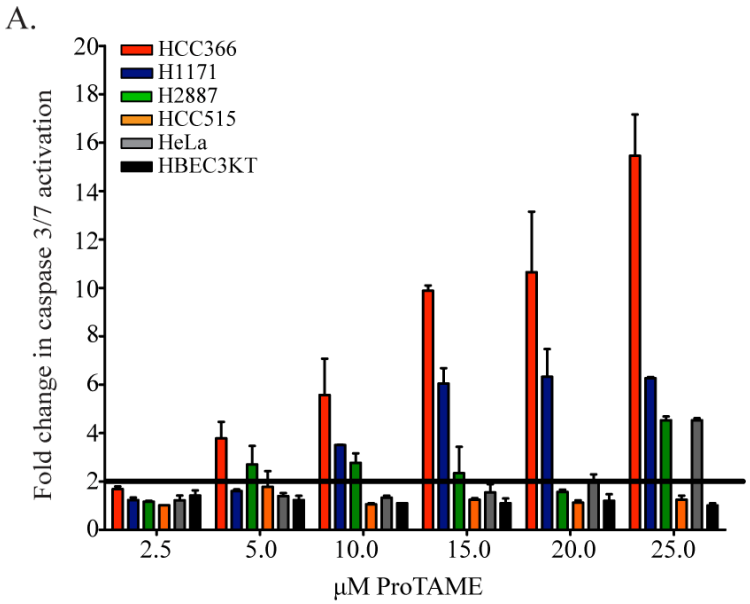

Figure 17: Slippage prone cell lines are most sensitive to APC/C inhibition

Indicated cell lines were treated with escalating doses of proTAME for 24 hours and assessed for caspase -3/7 activity using APO-ONE. Bar represents mean of 3 independent replicates. Error bar represents standard deviation.

REFERENCES

1. Siegel, R., D. Naishadham, and A. Jemal, *Cancer statistics, 2013.* CA Cancer J Clin, 2013. **63**(1): p. 11-30.

2. Herbst, R.S., J.V. Heymach, and S.M. Lippman, *Lung cancer.* N Engl J Med, 2008. **359**(13): p. 1367-80.

3. Larsen, J.E. and J.D. Minna, *Molecular biology of lung cancer: clinical implications.* Clin Chest Med, 2011. **32**(4): p. 703-40.

4. Boch, C., et al., *The frequency of EGFR and KRAS mutations in non-small cell lung cancer (NSCLC): routine screening data for central Europe from a cohort study.* BMJ Open, 2013. **3**(4).

5. Li, T., et al., *Genotyping and genomic profiling of non-small-cell lung cancer: implications for current and future therapies.* J Clin Oncol, 2013. **31**(8): p. 1039-49.

6. Maemondo, M., et al., *Gefitinib or chemotherapy for non-small-cell lung cancer with mutated EGFR.* N Engl J Med, 2010. **362**(25): p. 2380-8.

7. Mitsudomi, T., et al., *Gefitinib versus cisplatin plus docetaxel in patients with non-small-cell lung cancer harbouring mutations of the epidermal growth factor receptor (WJTOG3405): an open label, randomised phase 3 trial.* Lancet Oncol, 2010. **11**(2): p. 121-8.

8. Mok, T.S., et al., *Gefitinib or carboplatin-paclitaxel in pulmonary adenocarcinoma.* N Engl J Med, 2009. **361**(10): p. 947-57.

9. Rosell, R., et al., *Erlotinib versus standard chemotherapy as first-line treatment for European patients with advanced EGFR mutation-positive non-small-cell lung cancer (EURTAC): a multicentre, open-label, randomised phase 3 trial.* Lancet Oncol, 2012. **13**(3): p. 239-46.

10. Zhou, C., et al., *Erlotinib versus chemotherapy as first-line treatment for patients with advanced EGFR mutation-positive non-small-cell lung cancer (OPTIMAL, CTONG-0802): a multicentre, open-label, randomised, phase 3 study.* Lancet Oncol, 2011. **12**(8): p. 735-42.

11. Soda, M., et al., *Identification of the transforming EML4-ALK fusion gene in non-small-cell lung cancer.* Nature, 2007. **448**(7153): p. 561-6.

12. Solomon, B., M. Varella-Garcia, and D.R. Camidge, *ALK gene rearrangements: a new therapeutic target in a molecularly defined subset of non-small cell lung cancer.* J Thorac Oncol, 2009. **4**(12): p. 1450-4.

13. Kwak, E.L., et al., *Anaplastic lymphoma kinase inhibition in non-small-cell lung*

cancer. N Engl J Med, 2010. **363**(18): p. 1693-703.

14. Pfister, D.G., et al., *American Society of Clinical Oncology treatment of unresectable non-small-cell lung cancer guideline: update 2003.* J Clin Oncol, 2004. **22**(2): p. 330-53.

15. Schiller, J.H., et al., *Comparison of four chemotherapy regimens for advanced non-small-cell lung cancer.* N Engl J Med, 2002. **346**(2): p. 92-8.

16. Ichiki, M., et al., *A multicenter phase II study of carboplatin and paclitaxel with a biweekly schedule in patients with advanced non-small-cell lung cancer: Kyushu thoracic oncology group trial.* Cancer Chemother Pharmacol, 2006. **58**(3): p. 368-73.

17. McGuire, W.P., et al., *Taxol: a unique antineoplastic agent with significant activity in advanced ovarian epithelial neoplasms.* Ann Intern Med, 1989. **111**(4): p. 273-9.

18. Yumuk, P.F., et al., *Results of paclitaxel (day 1 and 8) and carboplatin given on every three weeks in advanced (stage III-IV) non-small cell lung cancer*. BMC Cancer, 2005. **5**: p. 10.

19. Zalcberg, J., et al., *Phase II study of docetaxel and cisplatin in advanced non-small-cell lung cancer*. J Clin Oncol, 1998. **16**(5): p. 1948-53.

20. Cragg, G.M., *Natural product drug discovery and development: the United States National Cancer Institute role.* P R Health Sci J, 2002. **21**(2): p. 97-111.

21. Rowinsky, E.K. and R.C. Donehower, *Paclitaxel (taxol).* N Engl J Med, 1995. **332**(15): p. 1004-14.

22. Wani, M.C., et al., *Plant antitumor agents. VI. The isolation and structure of taxol, a novel antileukemic and antitumor agent from Taxus brevifolia.* J Am Chem Soc, 1971. **93**(9): p. 2325-7.

23. Sarosy, G., et al., *Phase I study of taxol and granulocyte colony-stimulating factor in patients with refractory ovarian cancer.* J Clin Oncol, 1992. **10**(7): p. 1165-70.

24. Kohn, E.C., et al., *Dose-intense taxol: high response rate in patients with platinum-resistant recurrent ovarian cancer.* J Natl Cancer Inst, 1994. **86**(1): p. 18-24.

25. Rowinsky, E.K., et al., *Sequences of taxol and cisplatin: a phase I and pharmacologic study.* J Clin Oncol, 1991. **9**(9): p. 1692-703.

26. Finkelstein, D.M., D.S. Ettinger, and J.C. Ruckdeschel, *Long-term survivors in metastatic non-small-cell lung cancer: an Eastern Cooperative Oncology Group Study*. J Clin Oncol, 1986. **4**(5): p. 702-9.

27. Holmes, F.A., et al., *Phase II trial of taxol, an active drug in the treatment of metastatic breast cancer.* J Natl Cancer Inst, 1991. **83**(24): p. 1797-805.

28. Schiff, P.B., J. Fant, and S.B. Horwitz, *Promotion of microtubule assembly in vitro by taxol.* Nature, 1979. **277**(5698): p. 665-7.

29. Schiff, P.B. and S.B. Horwitz, *Taxol stabilizes microtubules in mouse fibroblast cells.* Proc Natl Acad Sci U S A, 1980. **77**(3): p. 1561-5.

30. Akhmanova, A. and M.O. Steinmetz, *Tracking the ends: a dynamic protein network controls the fate of microtubule tips.* Nat Rev Mol Cell Biol, 2008. **9**(4): p. 309-22.

31. Jordan, M.A. and K. Kamath, *How do microtubule-targeted drugs work? An overview.* Curr Cancer Drug Targets, 2007. **7**(8): p. 730-42.

32. Nogales, E., *Structural insights into microtubule function.* Annu Rev Biochem, 2000. **69**: p. 277-302.

33. Derry, W.B., L. Wilson, and M.A. Jordan, *Substoichiometric binding of taxol suppresses microtubule dynamics.* Biochemistry, 1995. **34**(7): p. 2203-11.

34. Derry, W.B., et al., *Taxol differentially modulates the dynamics of microtubules assembled from unfractionated and purified beta-tubulin isotypes.* Biochemistry, 1997. **36**(12): p. 3554-62.

35. Fuchs, D.A. and R.K. Johnson, *Cytologic evidence that taxol, an antineoplastic agent from Taxus brevifolia, acts as a mitotic spindle poison.* Cancer Treat Rep, 1978. **62**(8): p. 1219-22.

36. Hayden, J.H., S.S. Bowser, and C.L. Rieder, *Kinetochores capture astral microtubules during chromosome attachment to the mitotic spindle: direct visualization in live newt lung cells.* J Cell Biol, 1990. **111**(3): p. 1039-45.

37. Salmon, E.D., et al., *Merotelic kinetochores in mammalian tissue cells.* Philos Trans R Soc Lond B Biol Sci, 2005. **360**(1455): p. 553-68.

38. Maddox, P., et al., *Poleward microtubule flux is a major component of spindle dynamics and anaphase a in mitotic Drosophila embryos.* Curr Biol, 2002. **12**(19): p. 1670-4.

39. Mitchison, T.J., *Polewards microtubule flux in the mitotic spindle: evidence from photoactivation of fluorescence.* J Cell Biol, 1989. **109**(2): p. 637-52.

40. Hwang, L.H., et al., *Budding yeast Cdc20: a target of the spindle checkpoint.* Science, 1998. **279**(5353): p. 1041-4.

41. Musacchio, A. and E.D. Salmon, *The spindle-assembly checkpoint in space and*

time. Nat Rev Mol Cell Biol, 2007. **8**(5): p. 379-93.

42. Sudakin, V., G.K. Chan, and T.J. Yen, *Checkpoint inhibition of the APC/C in HeLa cells is mediated by a complex of BUBR1, BUB3, CDC20, and MAD2.* J Cell Biol, 2001. **154**(5): p. 925-36.

43. Howell, B.J., et al., *Cytoplasmic dynein/dynactin drives kinetochore protein transport to the spindle poles and has a role in mitotic spindle checkpoint inactivation.* J Cell Biol, 2001. **155**(7): p. 1159-72.

44. Waters, J.C., et al., *Localization of Mad2 to kinetochores depends on microtubule attachment, not tension.* J Cell Biol, 1998. **141**(5): p. 1181-91.

45. Rieder, C.L., et al., *The checkpoint delaying anaphase in response to chromosome monoorientation is mediated by an inhibitory signal produced by unattached kinetochores.* J Cell Biol, 1995. **130**(4): p. 941-8.

46. Siegel, J.J. and A. Amon, *New insights into the troubles of aneuploidy.* Annu Rev Cell Dev Biol, 2012. **28**: p. 189-214.

47. Weaver, B.A. and D.W. Cleveland, *Does aneuploidy cause cancer?* Curr Opin Cell Biol, 2006. **18**(6): p. 658-67.

48. Verweij, J., M. Clavel, and B. Chevalier, *Paclitaxel (Taxol) and docetaxel (Taxotere): not simply two of a kind.* Ann Oncol, 1994. **5**(6): p. 495-505.

49. Gascoigne, K.E. and S.S. Taylor, *How do anti-mitotic drugs kill cancer cells?* J Cell Sci, 2009. **122**(Pt 15): p. 2579-85.

50. McGrogan, B.T., et al., *Taxanes, microtubules and chemoresistant breast cancer.* Biochim Biophys Acta, 2008. **1785**(2): p. 96-132.

51. Ibrado, A.M., et al., *Bcl-xL overexpression inhibits taxol-induced Yama protease activity and apoptosis.* Cell Growth Differ, 1996. **7**(8): p. 1087-94.

52. Yusuf, R.Z., et al., *Paclitaxel resistance: molecular mechanisms and pharmacologic manipulation.* Curr Cancer Drug Targets, 2003. **3**(1): p. 1-19.

53. Berrieman, H.K., M.J. Lind, and L. Cawkwell, *Do beta-tubulin mutations have a role in resistance to chemotherapy?* Lancet Oncol, 2004. **5**(3): p. 158-64.

54. Orr, G.A., et al., *Mechanisms of Taxol resistance related to microtubules.* Oncogene, 2003. **22**(47): p. 7280-95.

55. Verdier-Pinard, P., et al., *Analysis of tubulin isotypes and mutations from taxol-resistant cells by combined isoelectrofocusing and mass spectrometry.* Biochemistry, 2003. **42**(18): p. 5349-57.

56. Kavallaris, M., *Microtubules and resistance to tubulin-binding agents.* Nat Rev Cancer, 2010. **10**(3): p. 194-204.

57. Gascoigne, K.E. and S.S. Taylor, *Cancer cells display profound intra- and interline variation following prolonged exposure to antimitotic drugs.* Cancer Cell, 2008. **14**(2): p. 111-22.

58. Rieder, C.L. and H. Maiato, *Stuck in division or passing through: what happens when cells cannot satisfy the spindle assembly checkpoint.* Dev Cell, 2004. **7**(5): p. 637-51.

59. Cahill, D.P., et al., *Mutations of mitotic checkpoint genes in human cancers.* Nature, 1998. **392**(6673): p. 300-3.

60. Brito, D.A. and C.L. Rieder, *Mitotic checkpoint slippage in humans occurs via cyclin B destruction in the presence of an active checkpoint.* Curr Biol, 2006. **16**(12): p. 1194-200.

61. Di Fiore, B. and J. Pines, *How cyclin A destruction escapes the spindle assembly checkpoint.* J Cell Biol, 2010. **190**(4): p. 501-9.

62. Foe, I.T., et al., *Ubiquitination of Cdc20 by the APC occurs through an intramolecular mechanism.* Curr Biol, 2011. **21**(22): p. 1870-7.

63. Geley, S., et al., *Anaphase-promoting complex/cyclosome-dependent proteolysis of human cyclin A starts at the beginning of mitosis and is not subject to the spindle assembly checkpoint.* J Cell Biol, 2001. **153**(1): p. 137-48.

64. Hames, R.S., et al., *APC/C-mediated destruction of the centrosomal kinase Nek2A occurs in early mitosis and depends upon a cyclin A-type D-box.* EMBO J, 2001. **20**(24): p. 7117-27.

65. Harley, M.E., et al., *Phosphorylation of Mcl-1 by CDK1-cyclin B1 initiates its Cdc20-dependent destruction during mitotic arrest.* EMBO J, 2010. **29**(14): p. 2407-20.

66. Wertz, I.E., et al., *Sensitivity to antitubulin chemotherapeutics is regulated by MCL1 and FBW7.* Nature, 2011. **471**(7336): p. 110-4.

67. Bekier, M.E., et al., *Length of mitotic arrest induced by microtubule-stabilizing drugs determines cell death after mitotic exit.* Mol Cancer Ther, 2009. **8**(6): p. 1646-54.

68. Cappell, K.M., et al., *Symplekin specifies mitotic fidelity by supporting microtubule dynamics.* Mol Cell Biol, 2010. **30**(21): p. 5135-44.

69. Cappell, K.M., et al., *Multiple cancer testes antigens function to support tumor cell mitotic fidelity.* Molecular and cellular biology, 2012. **32**(20): p. 4131-4140.

70. Whitehurst, A.W., et al., *Tumor antigen acrosin binding protein normalizes mitotic spindle function to promote cancer cell proliferation.* Cancer Res, 2010. **70**(19): p. 7652-61.

71. Whitehurst, A.W., et al., *Synthetic lethal screen identification of chemosensitizer loci in cancer cells.* Nature, 2007. **446**(7137): p. 815-9.

72. Cerami, E., et al., *The cBio cancer genomics portal: an open platform for exploring multidimensional cancer genomics data.* Cancer discovery, 2012. **2**(5): p. 401-4.

73. Cancer Genome Atlas Research, N., *Comprehensive genomic characterization of squamous cell lung cancers.* Nature, 2012. **489**(7417): p. 519-25.

74. Ward, S.E., et al., *Host modulators of H1N1 cytopathogenicity.* PLoS One, 2012. **7**(8): p. e39284.

75. Das, B., et al., *Nuclear co-translocation of myotrophin and p65 stimulates myocyte growth. Regulation by myotrophin hairpin loops.* J Biol Chem, 2008. **283**(41): p. 27947-56.

76. Al-Sohaily, S., et al., *Loss of Special AT-Rich Sequence-Binding Protein 1 (SATB1) Predicts Poor Survival in Patients with Colorectal Cancer.* Histopathology, 2013.

77. Han, S., et al., *Phosphorylated SATB1 is associated with the progression and prognosis of glioma.* Cell Death Dis, 2013. **4**: p. e901.

78. Shen, Z., et al., *Over-expression of the special AT rich sequence binding protein 1 (SATB1) promotes the progression of nasopharyngeal carcinoma: association with EBV LMP-1 expression.* J Transl Med, 2013. **11**(1): p. 217.

79. Lewis, S.A., G. Tian, and N.J. Cowan, *The alpha- and beta-tubulin folding pathways.* Trends Cell Biol, 1997. **7**(12): p. 479-84.

80. Prota, A.E., et al., *Structural basis of tubulin tyrosination by tubulin tyrosine ligase.* J Cell Biol, 2013. **200**(3): p. 259-70.

81. Schreiber, A., et al., *Structural basis for the subunit assembly of the anaphase-promoting complex.* Nature, 2011. **470**(7333): p. 227-32.

82. Poliseno, L., *Pseudogenes: newly discovered players in human cancer.* Sci Signal, 2012. **5**(242): p. re5.

83. Liu, P., et al., *Candidate lung tumor susceptibility genes identified through whole-genome association analyses in inbred mice.* Nat Genet, 2006. **38**(8): p. 888-95.

84. Uzawa, K., et al., *Targeting phosphodiesterase 3B enhances cisplatin sensitivity*

in human cancer cells. Cancer Med, 2013. **2**(1): p. 40-9.

85. Han, Y., et al., *Characterisation of human RING finger protein TRIM69, a novel testis E3 ubiquitin ligase and its subcellular localisation.* Biochem Biophys Res Commun, 2012. **429**(1-2): p. 6-11.

86. Zhong, Q., et al., *Mule/ARF-BP1, a BH3-only E3 ubiquitin ligase, catalyzes the polyubiquitination of Mcl-1 and regulates apoptosis.* Cell, 2005. **121**(7): p. 1085-95.

87. Zeng, X., et al., *Pharmacologic inhibition of the anaphase-promoting complex induces a spindle checkpoint-dependent mitotic arrest in the absence of spindle damage.* Cancer Cell, 2010. **18**(4): p. 382-95.

88. Sellers, T.A., et al., *Evidence for mendelian inheritance in the pathogenesis of lung cancer.* J Natl Cancer Inst, 1990. **82**(15): p. 1272-9.

89. Sellers, T.A., et al., *Lung cancer histologic type and family history of cancer.* Cancer, 1992. **69**(1): p. 86-91.

90. Sellers, T.A., J.D. Potter, and A.R. Folsom, *Association of incident lung cancer with family history of female reproductive cancers: the Iowa Women's Health Study.* Genet Epidemiol, 1991. **8**(3): p. 199-208.

91. Gariboldi, M., et al., *A major susceptibility locus to murine lung carcinogenesis maps on chromosome 6.* Nat Genet, 1993. **3**(2): p. 132-6.

92. Malkinson, A.M. and D.S. Beer, *Major effect on susceptibility to urethan-induced pulmonary adenoma by a single gene in BALB/cBy mice.* J Natl Cancer Inst, 1983. **70**(5): p. 931-6.

93. Zhang, Z., et al., *Positional cloning of the major quantitative trait locus underlying lung tumor susceptibility in mice.* Proc Natl Acad Sci U S A, 2003. **100**(22): p. 12642-7.

94. Galbiati, F., et al., *Allelic effects of mouse Pas1 candidate genes in human lung cancer cell lines.* Cancer Lett, 2006. **244**(2): p. 176-81.

95. Liu, Y., et al., *Degradation of lung adenoma susceptibility 1, a major candidate mouse lung tumor modifier, is required for cell cycle progression.* Cancer Res, 2007. **67**(21): p. 10207-13.

96. Sato, M., et al., *Multiple oncogenic changes (K-RAS(V12), p53 knockdown, mutant EGFRs, p16 bypass, telomerase) are not sufficient to confer a full malignant phenotype on human bronchial epithelial cells.* Cancer Res, 2006. **66**(4): p. 2116-28.

97. Cappell, K.M., et al., *Multiple cancer testis antigens function to support tumor*

cell mitotic fidelity. Mol Cell Biol, 2012. **32**(20): p. 4131-40.

98. Luo, J., et al., *A genome-wide RNAi screen identifies multiple synthetic lethal interactions with the Ras oncogene.* Cell, 2009. **137**(5): p. 835-48.

99. Wagner, P.L., et al., *Frequency and clinicopathologic correlates of KRAS amplification in non-small cell lung carcinoma.* Lung Cancer, 2011. **74**(1): p. 118-23.

100. Coschi, C.H., et al., *Mitotic chromosome condensation mediated by the retinoblastoma protein is tumor-suppressive.* Genes Dev, 2010. **24**(13): p. 1351-63.

101. Hergovich, A., et al., *Regulation of microtubule stability by the von Hippel-Lindau tumour suppressor protein pVHL.* Nat Cell Biol, 2003. **5**(1): p. 64-70.

102. Liu, L., et al., *Control of microtubule stability by the RASSF1A tumor suppressor.* Oncogene, 2003. **22**(50): p. 8125-36.

103. Manning, A.L., M.S. Longworth, and N.J. Dyson, *Loss of pRB causes centromere dysfunction and chromosomal instability.* Genes Dev, 2010. **24**(13): p. 1364-76.

104. van Harn, T., et al., *Loss of Rb proteins causes genomic instability in the absence of mitogenic signaling.* Genes Dev, 2010. **24**(13): p. 1377-88.

105. Andreassen, P.R., et al., *Tetraploid state induces p53-dependent arrest of nontransformed mammalian cells in G1.* Mol Biol Cell, 2001. **12**(5): p. 1315-28.

106. Ditchfield, C., et al., *Aurora B couples chromosome alignment with anaphase by targeting BubR1, Mad2, and Cenp-E to kinetochores.* J Cell Biol, 2003. **161**(2): p. 267-80.

107. Lanni, J.S. and T. Jacks, *Characterization of the p53-dependent postmitotic checkpoint following spindle disruption.* Mol Cell Biol, 1998. **18**(2): p. 1055-64.

108. Giannakakou, P., et al., *Low concentrations of paclitaxel induce cell type-dependent p53, p21 and G1/G2 arrest instead of mitotic arrest: molecular determinants of paclitaxel-induced cytotoxicity.* Oncogene, 2001. **20**(29): p. 3806-13.

109. Wahl, A.F., et al., *Loss of normal p53 function confers sensitization to Taxol by increasing G2/M arrest and apoptosis.* Nat Med, 1996. **2**(1): p. 72-9.

110. Brito, D.A., Z. Yang, and C.L. Rieder, *Microtubules do not promote mitotic slippage when the spindle assembly checkpoint cannot be satisfied.* J Cell Biol, 2008. **182**(4): p. 623-9.

111. Collin, P., et al., *The spindle assembly checkpoint works like a rheostat rather*

than a toggle switch. Nat Cell Biol, 2013. **15**(11): p. 1378-85.

112. Yang, Z., et al., *Cells satisfy the mitotic checkpoint in Taxol, and do so faster in concentrations that stabilize syntelic attachments.* J Cell Biol, 2009. **186**(5): p. 675-84.

113. Dick, A.E. and D.W. Gerlich, *Kinetic framework of spindle assembly checkpoint signalling.* Nat Cell Biol, 2013. **15**(11): p. 1370-7.

114. Heinrich, S., et al., *Determinants of robustness in spindle assembly checkpoint signalling.* Nat Cell Biol, 2013. **15**(11): p. 1328-39.

115. Hatakeyama, S., *TRIM proteins and cancer.* Nat Rev Cancer, 2011. **11**(11): p. 792-804.

116. Nisole, S., J.P. Stoye, and A. Saib, *TRIM family proteins: retroviral restriction and antiviral defence.* Nat Rev Microbiol, 2005. **3**(10): p. 799-808.

117. Meroni, G. and G. Diez-Roux, *TRIM/RBCC, a novel class of 'single protein RING finger' E3 ubiquitin ligases.* Bioessays, 2005. **27**(11): p. 1147-57.

118. Teixeira, L.K. and S.I. Reed, *Ubiquitin ligases and cell cycle control.* Annu Rev Biochem, 2013. **82**: p. 387-414.

119. Metzger, M.B., V.A. Hristova, and A.M. Weissman, *HECT and RING finger families of E3 ubiquitin ligases at a glance.* J Cell Sci, 2012. **125**(Pt 3): p. 531-7.

120. Chen, A., et al., *The conserved RING-H2 finger of ROC1 is required for ubiquitin ligation.* J Biol Chem, 2000. **275**(20): p. 15432-9.

121. Du, H., et al., *The MID1 E3 ligase catalyzes the polyubiquitination of Alpha4 (alpha4), a regulatory subunit of protein phosphatase 2A (PP2A): novel insights into MID1-mediated regulation of PP2A.* J Biol Chem, 2013. **288**(29): p. 21341-50.

122. Schweiger, S. and R. Schneider, *The MID1/PP2A complex: a key to the pathogenesis of Opitz BBB/G syndrome.* Bioessays, 2003. **25**(4): p. 356-66.

123. Goddard, A.D., J. Borrow, and E. Solomon, *A previously uncharacterized gene, PML, is fused to the retinoic acid receptor alpha gene in acute promyelocytic leukaemia.* Leukemia, 1992. **6 Suppl 3**: p. 117S-119S.

124. Doyle, J.M., et al., *MAGE-RING protein complexes comprise a family of E3 ubiquitin ligases.* Mol Cell, 2010. **39**(6): p. 963-74.

125. Whitehurst, A.W., *Cause and Consequence of Cancer/Testis Antigen Activation in Cancer.* Annu Rev Pharmacol Toxicol, 2013.

126. Shyu, H.W., et al., *A novel member of the RBCC family, Trif, expressed specifically in the spermatids of mouse testis.* Mech Dev, 2001. **108**(1-2): p. 213-6.

127. Cho, H. and J.H. Kehrl, *Localization of Gi alpha proteins in the centrosomes and at the midbody: implication for their role in cell division.* J Cell Biol, 2007. **178**(2): p. 245-55.

128. Chiyoda, T., et al., *LATS1/WARTS phosphorylates MYPT1 to counteract PLK1 and regulate mammalian mitotic progression.* J Cell Biol, 2012. **197**(5): p. 625-41.

129. Liu, D., et al., *Regulated targeting of protein phosphatase 1 to the outer kinetochore by KNL1 opposes Aurora B kinase.* J Cell Biol, 2010. **188**(6): p. 809-20.

130. Posch, M., et al., *Sds22 regulates aurora B activity and microtubule-kinetochore interactions at mitosis.* J Cell Biol, 2010. **191**(1): p. 61-74.

131. Yamashiro, S., et al., *Myosin phosphatase-targeting subunit 1 regulates mitosis by antagonizing polo-like kinase 1.* Dev Cell, 2008. **14**(5): p. 787-97.

132. Peikert, T., et al., *Melanoma antigen A4 is expressed in non-small cell lung cancers and promotes apoptosis.* Cancer Res, 2006. **66**(9): p. 4693-700.

133. Starita, L.M., et al., *BRCA1-dependent ubiquitination of gamma-tubulin regulates centrosome number.* Mol Cell Biol, 2004. **24**(19): p. 8457-66.

134. Beck, J. and M. Peter, *Regulating PLK1 dynamics by Cullin3/KLHL22-mediated ubiquitylation.* Cell Cycle, 2013. **12**(16): p. 2528-9.

135. Beck, J., et al., *Ubiquitylation-dependent localization of PLK1 in mitosis.* Nat Cell Biol, 2013. **15**(4): p. 430-9.

136. Piehl, M., et al., *Centrosome maturation: measurement of microtubule nucleation throughout the cell cycle by using GFP-tagged EB1.* Proc Natl Acad Sci U S A, 2004. **101**(6): p. 1584-8.

137. Palazzo, R.E., et al., *Centrosome maturation.* Curr Top Dev Biol, 2000. **49**: p. 449-70.

138. Albee, A.J. and C. Wiese, *Xenopus TACC3/maskin is not required for microtubule stability but is required for anchoring microtubules at the centrosome.* Mol Biol Cell, 2008. **19**(8): p. 3347-56.

139. Delgehyr, N., J. Sillibourne, and M. Bornens, *Microtubule nucleation and anchoring at the centrosome are independent processes linked by ninein function.* J Cell Sci, 2005. **118**(Pt 8): p. 1565-75.

140. Hendrickx, A., et al., *Docking motif-guided mapping of the interactome of protein phosphatase-1.* Chem Biol, 2009. **16**(4): p. 365-71.

141. Lesage, B., J. Qian, and M. Bollen, *Spindle checkpoint silencing: PP1 tips the balance.* Curr Biol, 2011. **21**(21): p. R898-903.

142. Huang, H.C., et al., *Evidence that mitotic exit is a better cancer therapeutic target than spindle assembly.* Cancer Cell, 2009. **16**(4): p. 347-58.

143. Carbonaro, M., A. O'Brate, and P. Giannakakou, *Microtubule disruption targets HIF-1alpha mRNA to cytoplasmic P-bodies for translational repression.* J Cell Biol, 2011. **192**(1): p. 83-99.

144. Thadani-Mulero, M., D.M. Nanus, and P. Giannakakou, *Androgen receptor on the move: boarding the microtubule expressway to the nucleus.* Cancer Res, 2012. **72**(18): p. 4611-5.

145. Roth, D.M., et al., *A microtubule-facilitated nuclear import pathway for cancer regulatory proteins.* Traffic, 2007. **8**(6): p. 673-86.

146. Giannakakou, P., et al., *Enhanced microtubule-dependent trafficking and p53 nuclear accumulation by suppression of microtubule dynamics.* Proc Natl Acad Sci U S A, 2002. **99**(16): p. 10855-60.

147. Mitchison, T.J., *The proliferation rate paradox in antimitotic chemotherapy.* Mol Biol Cell, 2012. **23**(1): p. 1-6.

148. Koga, Y. and M. Ikebe, *p116Rip decreases myosin II phosphorylation by activating myosin light chain phosphatase and by inactivating RhoA.* J Biol Chem, 2005. **280**(6): p. 4983-91.

149. Kao, S.C., et al., *Identification of phostensin, a PP1 F-actin cytoskeleton targeting subunit.* Biochem Biophys Res Commun, 2007. **356**(3): p. 594-8.

150. Lai, N.S., et al., *Phostensin caps to the pointed end of actin filaments and modulates actin dynamics.* Biochem Biophys Res Commun, 2009. **387**(4): p. 676-81.

151. Wang, W., et al., *NELIN, a new F-actin associated protein, stimulates HeLa cell migration and adhesion.* Biochem Biophys Res Commun, 2005. **330**(4): p. 1127-31.

152. Lawo, S., et al., *HAUS, the 8-subunit human Augmin complex, regulates centrosome and spindle integrity.* Curr Biol, 2009. **19**(10): p. 816-26.

153. Maier, B., et al., *The novel actin/focal adhesion-associated protein MISP is involved in mitotic spindle positioning in human cells.* Cell Cycle, 2013. **12**(9): p. 1457-71.